

Article

Development of Small Molecules that Specifically Inhibit the D-loop Activity of RAD51

Wei Lv, Brian Budke, Michal Pawlowski, Philip P. Connell, and Alan P. Kozikowski

J. Med. Chem., **Just Accepted Manuscript** • DOI: 10.1021/acs.jmedchem.5b01762 • Publication Date (Web): 06 Apr 2016

Downloaded from <http://pubs.acs.org> on April 7, 2016

Just Accepted

“Just Accepted” manuscripts have been peer-reviewed and accepted for publication. They are posted online prior to technical editing, formatting for publication and author proofing. The American Chemical Society provides “Just Accepted” as a free service to the research community to expedite the dissemination of scientific material as soon as possible after acceptance. “Just Accepted” manuscripts appear in full in PDF format accompanied by an HTML abstract. “Just Accepted” manuscripts have been fully peer reviewed, but should not be considered the official version of record. They are accessible to all readers and citable by the Digital Object Identifier (DOI®). “Just Accepted” is an optional service offered to authors. Therefore, the “Just Accepted” Web site may not include all articles that will be published in the journal. After a manuscript is technically edited and formatted, it will be removed from the “Just Accepted” Web site and published as an ASAP article. Note that technical editing may introduce minor changes to the manuscript text and/or graphics which could affect content, and all legal disclaimers and ethical guidelines that apply to the journal pertain. ACS cannot be held responsible for errors or consequences arising from the use of information contained in these “Just Accepted” manuscripts.



ACS Publications

**Development of Small Molecules that Specifically Inhibit the D-loop Activity
of RAD51**

Wei Lv,^{†§} Brian Budke,^{‡§} Michal Pawlowski,[†] Philip P. Connell,^{‡||} and Alan P. Kozikowski^{†||}

[†]Department of Medicinal Chemistry and Pharmacognosy, Drug Discovery Program, University
of Illinois at Chicago, Chicago, Illinois 60612, United States

[‡]Department of Radiation and Cellular Oncology, University of Chicago, Chicago, Illinois
60637, United States

Abstract

RAD51 is the central protein in homologous recombination (HR) DNA repair and represents a therapeutic target in oncology. Herein we report a novel class of RAD51 inhibitors that were identified by high throughput screening. In contrast to many previously reported RAD51 inhibitors, our lead compound **1** is capable of blocking RAD51-mediated D-loop formation (IC_{50} $21.3 \pm 7.8 \mu M$) at concentrations that do not influence RAD51 binding to ssDNA. In human cells, **1** inhibits HR (IC_{50} $13.1 \pm 1.6 \mu M$) without blocking RAD51's ability to assemble into sub-nuclear foci at sites of DNA damage. We determined that the active constituent of **1** is actually an oxidized derivative (termed **RI(dl)-1** or **8**) of the original screening compound. Our SAR campaign also yielded **RI(dl)-2** (hereafter termed **9h**), which effectively blocks RAD51's D-loop activity in biochemical systems (IC_{50} $11.1 \pm 1.3 \mu M$) and inhibits HR activity in human cells (IC_{50} $3.0 \pm 1.8 \mu M$).

Introduction

Homologous recombination (HR) is an evolutionarily conserved DNA repair process, which repairs DNA double strand breaks (DSBs) and promotes tolerance of inter-strand DNA cross-links (ICLs). Unlike the error-prone non-homologous end-joining (NHEJ) pathway of DSB rejoining, HR faithfully repairs DNA damage by utilizing an undamaged homologous DNA template to guide the repair process.^{1, 2} An initial step of HR involves nuclease processing that generates a 3' single-stranded DNA (ssDNA) tail at the site of DNA damage (**Figure 1**). The ssDNA is then coated with RAD51 protein to form a helical nucleoprotein filament. This resulting nucleoprotein filament subsequently searches for a homologous DNA sequence and invades it to form a joint molecule intermediate, termed a D-loop. Finally, with the assistance of other related HR proteins, accurate DNA synthesis is performed using the undamaged homologous sequence as a template.

Since HR facilitates cellular recovery from harmful DNA lesions, cells with deficient HR functionality are especially vulnerable to radiotherapy and chemotherapeutic agents that generate DSBs or DNA replication-blocking lesions.²⁻⁴ RAD51, the central protein of HR, is over-expressed in various types of human cancer cells.^{5, 6} These high expression levels of RAD51 can elevate HR efficiency in cancer cells, thereby inducing cellular resistance to DNA-damaging chemotherapy and radiotherapy.⁷⁻¹⁰ Inhibition of RAD51 by antisense RNAs or RAD51 inhibitors are reported to enhance the sensitivity of cancer cells to chemotherapy and radiotherapy.¹¹⁻¹³ These observations support the concept of RAD51 as a therapeutic target and the development of small molecule therapeutics to sensitize tumors.¹⁴⁻¹⁶ Although several small molecule RAD51 inhibitors have been developed, most of these inhibitors act by preventing the formation of RAD51-ssDNA nucleoprotein filaments.^{13, 14, 16-19} One possible exception is

halenaquinone, a chemical purported to specifically inhibit D-loop formation by RAD51.²⁰ However, halenaquinone also reduces the sub-nuclear appearance of RAD51 foci at DSB sites in cells, which raises questions as to its mechanistic interaction with RAD51 in cells.

In addition to its function in HR, RAD51 filaments also serve an important function at stalled DNA replication forks.^{21, 22} These RAD51 nucleoprotein filaments protect the ssDNA from extensive nuclease processing, thereby aiding in replication and preserving genomic integrity. Since most RAD51 inhibitors act by preventing the formation of RAD51 nucleoprotein filaments on ssDNA, they are expected to inhibit both HR and replication fork stabilization activities of RAD51. As such, their use is predicted to generate unintended toxicity to normal cells by interrupting this centrally-important function in normal replication.

We reasoned that specifically inhibiting RAD51-mediated D-loop formation while preserving RAD51's ability to form nucleoprotein filaments may target DNA repair while minimizing replication-associated toxicity in normal tissue. Therefore, we carried out a two-part high-throughput (HT) screen of the ASDI diversity library and LOPAC1280 compound library for drug candidates that selectively target RAD51's D-loop function. The preferred lead compound resulting from this screen, compound **1**, inhibits RAD51's D-loop activity while having minimal effects on RAD51's ssDNA binding activity. Compound **1** is a commercially obtained sample labeled as 4-(7-methoxy-4,5-dihydropyrrolo[1,2-a]quinoxalin-4-yl)-*N,N*-dimethylaniline, but its structure was found to be inconsistent with the named compound. This report details our HT screen and subsequent structure-activity relationship (SAR) optimizations performed to improve the potency and selectivity of **1**.

Results and Discussion

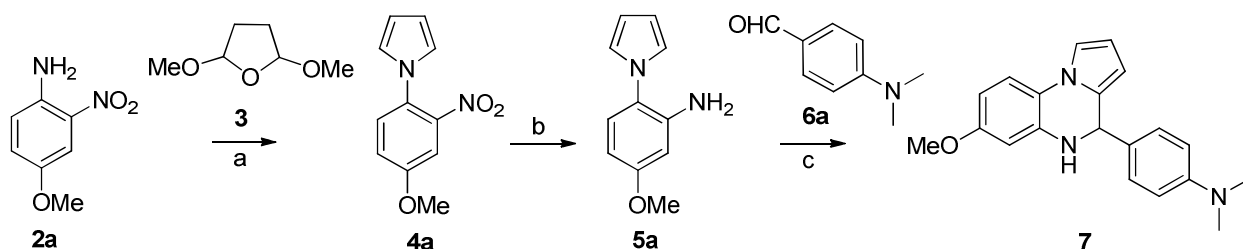
Screen for RAD51 D-loop inhibitors. We carried out two parallel HT screens to identify small molecules that inhibit RAD51 D-loop activity without affecting its ssDNA binding activity. A previously-described fluorescence polarization-based microplate assay was used to assess the compounds' effects on RAD51-ssDNA binding²³ (**Figure 2a**). In order to enable a screen for D-loop specific RAD51 inhibitors, we previously developed a microplate-based assay that can accurately quantify D-loop formation in a high-throughput fashion²⁴ (**Figure 2b**). This method makes use of two substrates: a closed linear double-hairpin dsDNA, and an ssDNA fused with a black hole quencher. The sequence homology of the two substrates enables RAD51 to catalyze the formation of D-loops, which is quantified as a function of quenched fluorescence. Among the screening compounds tested, we focused on those that prevented RAD51 D-loop formation while exerting little effect on RAD51-ssDNA binding (**Figure 2c**). Potential hits were confirmed using secondary low-throughput re-testing, which involved a gel-based D-loop assay to exclude the possibility that the observed inhibition of D-loop activity was due to artefactual interference by compound auto-fluorescence or fluorescence quenching.

Using this screening platform, the ASDI diversity library (6800 compounds of diverse chemical structures) and the LOPAC library of known drugs (library of 1280 pharmacologically active compounds) were screened, leading to the identification of 10 hit compounds that were capable of inhibiting D-loop activities with minimal effects on ssDNA binding. The best of these 10 compounds is shown in **Figure 3** and hereon referred to as **1**. Compound **1** inhibits the D-loop activity of RAD51 by up to 74%, while exerting minimal dose-dependent inhibition of RAD51

filament assembly in the same concentration range (**Figure 3**). As expected, parallel experiments demonstrate that the more generalized inhibitors of RAD51 (like RI-1) do generate dose-dependent inhibition of RAD51 filament assembly using identical assay conditions (see **Figure 7b** for reference).

Synthesis and activities of the reduced and oxidized forms of 1. As compound **1** was identified from a commercial compound library, we decided to first confirm its chemical structure by carrying out our own independent synthesis as detailed in **Scheme 1**. The starting material **2a** was first condensed with dimethoxytetrahydrofuran (**3**) in refluxing acetic acid to afford **4a**.²⁹ The nitro group of **4a** was then reduced, and the aniline **5a**²⁹ was reacted with benzaldehyde **6a** in the presence of 1,2,3-benzotriazole and AlCl₃ to provide the desired product **7** in moderate yield.

Scheme 1. Synthesis of **7**^a

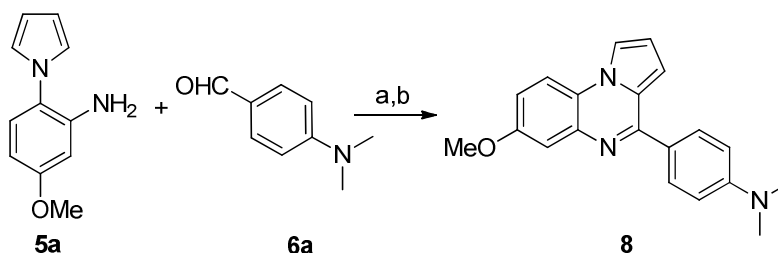


^aReagents and conditions: (a) AcOH, reflux, 3 h, 90%; (b) H₂, Pd/C, MeOH, 5 h, 97%; (c) 1,2,3-benzotriazole, AlCl₃, THF, 4 h, 32%.

The newly synthesized compound **7** was then subjected to biological evaluation as shown in **Table 1**. Unexpectedly, compound **7** displayed a much weaker D-loop inhibitory activity in comparison to the compound **1** that we obtained from the commercial source (maximum inhibition of 17% for **7** vs 74% for **1**). Moreover, compound **7** also showed significant

stimulatory activity in RAD51-ssDNA binding when compared to **1**. These discrepancies suggested that compound **7** and **1** might be different substances. Interestingly, we observed that compound **7** was not stable when exposed to air at room temperature; instead, it slowly oxidized over time to compound **8** (**Scheme 2**). Additionally, we found during the preparation of compound **7**, some of the oxidized product **8** was always produced. These observations raised the possibility that the commercially obtained material **1** might have undergone oxidation during its storage, and that the oxidized form **8** might be the active constituent responsible for the D-loop inhibitory activity of **1**.

To confirm this hypothesis, the structural identity of compound **1** was determined. According to the ^1H NMR spectrum, the commercially obtained material **1** was impure, with the oxidized compound **8** as the major component (**Figure S1**). The presence of compound **7** was not observed. The mass spectrum also confirmed the presence of compound **8** rather than compound **7**. To further confirm the D-loop inhibitory activity of this oxidized compound, compound **8** was synthesized by following the route as shown in **Scheme 2**. The aniline **5a** and benzaldehyde **6a** were reacted in the presence of 1,2,3-benzotriazole and AlCl_3 at room temperature until the conversion was complete, which resulted in a mixture of the reduced (**7**) and oxidized (**8**) forms. This crude mixture was then heated in acetone with MnO_2 to induce further oxidation, thereby yielding the oxidized form **8** as the exclusive product. Subsequent testing in our D-loop assay (**Table 1**) showed that compound **8** exhibits similar activity to **1** in terms of maximal inhibition (67% vs 74%, respectively) and IC_{50} values (13.0 vs 21.3 μM , respectively). These results thus confirm that the oxidized form **8** is the actual substance that generates the D-loop inhibitory activity of the commercially obtained compound **1**. Therefore, we have named compound **8** as “**RI(dl)-1**”, for D-loop activity of RAD51 Inhibitor #1.

Scheme 2. Synthesis of **8**^a

^aReagents and conditions: (a) 1,2,3-benzotriazole, AlCl₃, THF, overnight; (b) MnO₂, acetone, 55 °C, 24 h, 59% in two steps.

Table 1. The RAD51 D-loop inhibitory and RAD51-ssDNA binding stimulatory/inhibitory activities of **1**, **7** and **8**.

Cpd	D-Loops		ssDNA binding	
	Max inhibition effect	IC ₅₀ (μM)	Max effect	IC ₅₀ (μM)
1	74±2%	21.3±7.8	33±10%↓	>100
7	17±3%	>100	47±33%↑	Stim
8	67±11%	13.0±4.7	40±28%↑	Stim

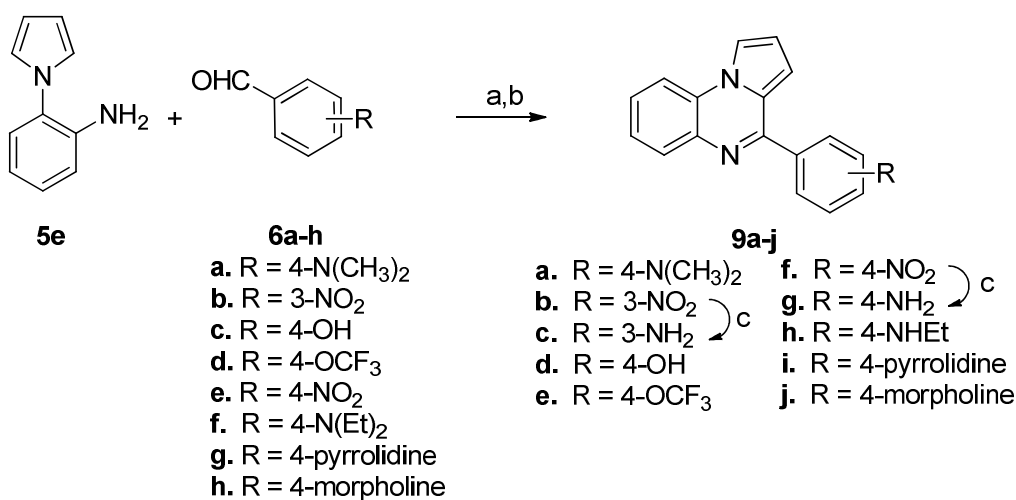
“↑” Indicates that the compound stimulates RAD51-ssDNA binding. “↓” Compound inhibits RAD51-ssDNA binding. “Stim” Compound is a stimulator.

Structure optimization of 8. To improve upon the D-loop inhibitory activity, medicinal chemical studies were undertaken to optimize **8**. An overview of the optimization strategy is summarized in **Figure 4**. First, different functional groups were appended to rings A and B as substituents, including alkyl groups of different sizes, electron withdrawing/donating groups, and hydrogen bond donor/acceptor groups. Next, replacement of the phenyl ring B with different heterocycles or other saturated/unsaturated rings was investigated in order to probe its role. For

each of the prepared compounds, we used the gel-based D-loop assay and the microplate-based DNA binding assay to characterize the biochemical activities.

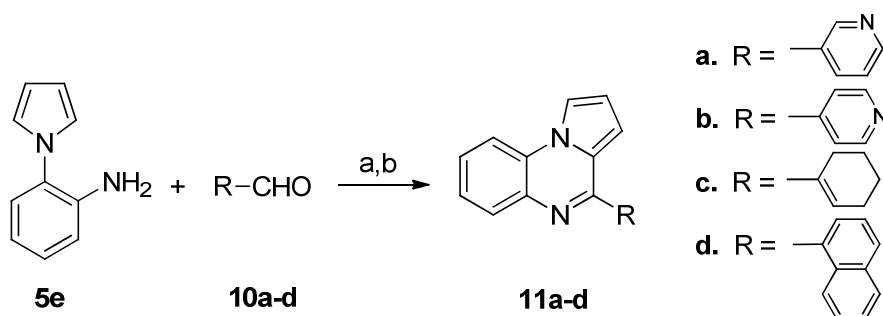
Optimization of ring B. To synthesize analogues with different substituents in the B-ring, the aniline **5e** was treated with different benzaldehydes **6a-h** in the presence of 1,2,3-benzotriazole and AlCl₃ (in **Scheme 3**). Then the crude products were oxidized with MnO₂ to provide **9a-j** in good yield. Interestingly, when benzaldehyde **6f** was reacted with the aniline **5e** under these conditions, partial de-ethylation was observed and the mono-ethylated product **9h** was isolated as the major product. The analogues **9c** and **9g** were obtained by reducing the nitro group of **9b** and **9f**³¹ via hydrogenation. To synthesize analogues in which the B-ring was replaced with other aromatic or saturated rings, the aniline **5e** was reacted with different aldehydes **10a-d** under similar conditions (in **Scheme 4**) to afford the products **11a-d**³¹⁻³³ in good yield.

Scheme 3. Synthesis of Analogues **9a-j**^a



^aReagents and conditions: (a) 1,2,3-benzotriazole, AlCl₃, THF, overnight; (b) MnO₂, acetone, 55

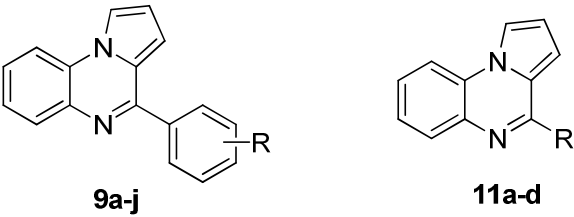
°C, 24 h, 19-70% in two steps; (c) H₂, Pd/C, methanol, 5h, 57-87%.

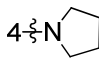
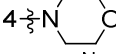
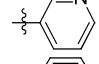
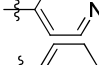
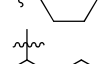
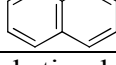
Scheme 4. Synthesis of Analogues **11a-d**^a

^aReagents and conditions: (a) 1,2,3-benzotriazole, AlCl₃, THF, overnight; (b) MnO₂, acetone, 55 °C, 24 h, 35-71% in two steps.

The D-loop inhibitory activities measured for compounds **9a-j** and **11a-d** are shown in **Table 2** (see D-loop gels in **Figure S2**). Results indicate that a dimethylamino group (**9a**), amino group (**9g**), ethylamino group (**9h**) or morpholine ring (**9j**) in the para position of the B-ring allow for D-loop inhibition, and that **9g** and **9h** display potencies that are similar to that of compound **8**. By contrast, introducing a hydroxyl group (**9d**), trifluoromethoxyl group (**9e**), nitro group (**9f**), or pyrrolidine group (**9i**) in the para-position significantly decreased the D-loop inhibitory activities. Moving the amino group from the para- (**9g**) to the meta-position (**9c**) also decreased the D-loop inhibitory activity. Replacing the B-ring with other aromatic or saturated rings only resulted in moderate (**11a**, **11b**) or weak (**11c**, **11d**) D-loop inhibitors. The ability of these analogs to modulate RAD51's ssDNA binding was also evaluated as shown in **Table 2**. Many of these compounds had only a weak influence on RAD51-ssDNA binding. On the other hand, compounds **9a**, **9b**, **9i**, **11c**, and **11d** had a modest influence on RAD51-ssDNA binding.

Table 2. The RAD51 D-loop inhibitory and RAD51-ssDNA binding stimulatory/inhibitory activities of **9a-j** and **11a-d**.



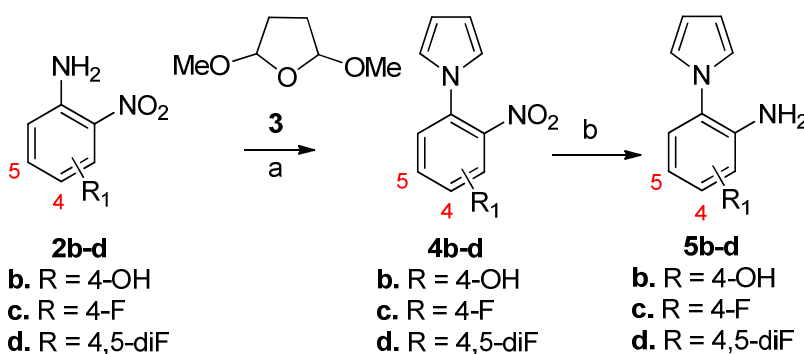
Cpd	R	D-Loops		ssDNA binding	
		Max inhibition effect	IC ₅₀ (μM)	Max effect	IC ₅₀ (μM)
9a	4-N(CH ₃) ₂	61±4%	27.6±6.0	88±22%↑	Stim
9b	3-NO ₂	20±8%	>100	52±14%↓	>100
9c	3-NH ₂	79±8%	91.1±10.3	11±9%↓	>100
9d	4-OH	38±3%	>100	14±16%↓	>100
9e	4-OCF ₃	22±8%	>100	30±21%↑	Stim
9f	4-NO ₂	2±21%	>100	16±13%↓	>100
9g	4-NH ₂	100±2%	22.1±2.4	18±11%↓	>100
9h	4-NHEt	91±1%	11.1±1.3	2±24%↑	>100
9i		8±7%	>100	69±35%↑	Stim
9j		68±7%	27.2±3.0	11±19%↓	>100
11a		70±13%	71.7±18.1	6±10%↓	>100
11b		63±4%	79.4±6.0	7±38%↓	>100
11c		5±11%	>100	42±17%↑	Stim
11d		42±11%	>100	56±31%↑	Stim

“↑” Compound stimulates RAD51-ssDNA binding. “↓”Compound inhibits RAD51-ssDNA binding. “Stim” Compound is a stimulator.

Optimization of ring A. To synthesize analogues with different substituents in the A-ring, the substituted anilines **5b-d** were first prepared according to the route shown in **Scheme 5**. The starting materials **2b-d** were condensed with dimethoxytetrahydrofuran (**3**) in refluxing acetic

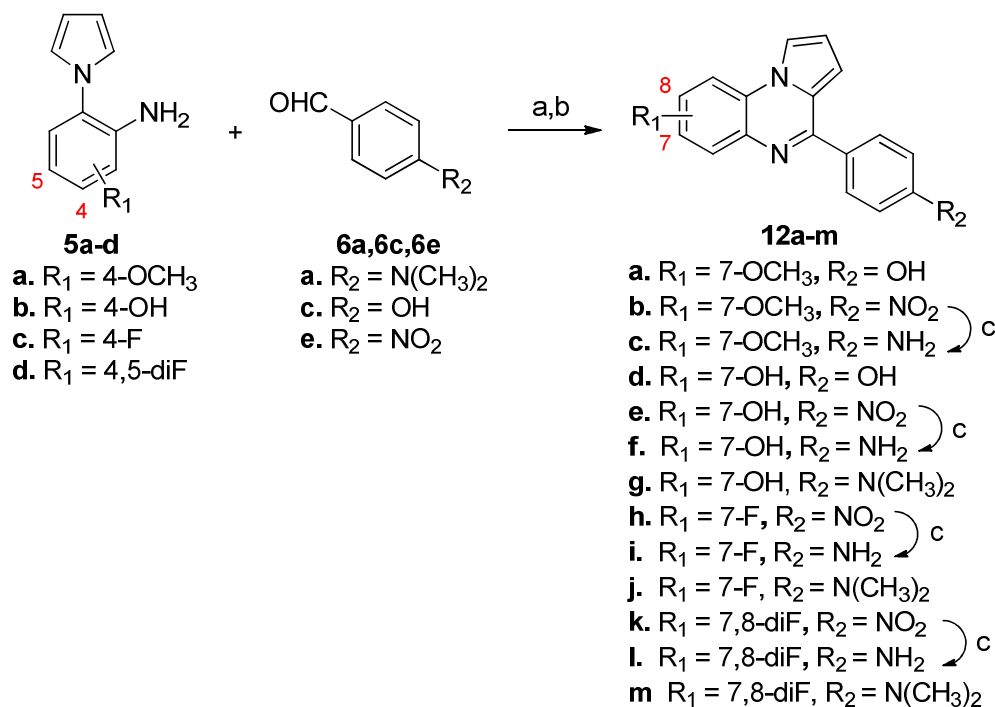
acid to afford **4b-d**.³⁰ Then, the nitro group was reduced to provide the products **5b-d**. Subsequently, the anilines **5a-d** were reacted with benzaldehydes (**6a**, **6c** and **6e**) to provide the analogues **12a-m** in good yield (in **Scheme 6**). For analogues with an amino group (**12c**, **12f**, **12i** and **12l**), compounds were prepared from the corresponding nitro analogues (**12b**, **12e**, **12h**, **12k**) via hydrogenation. Two analogues (**13a-b**) with a 3-pyridine ring were also prepared from anilines **5a-b** and aldehyde **10a** as shown in **Scheme 7**.

Scheme 5. Synthesis of 5b-d^a



Reagents and conditions: (a) AcOH, reflux, 3 h, 45-63%; (b) H₂, Pd/C, MeOH, 5 h, 37-97%.

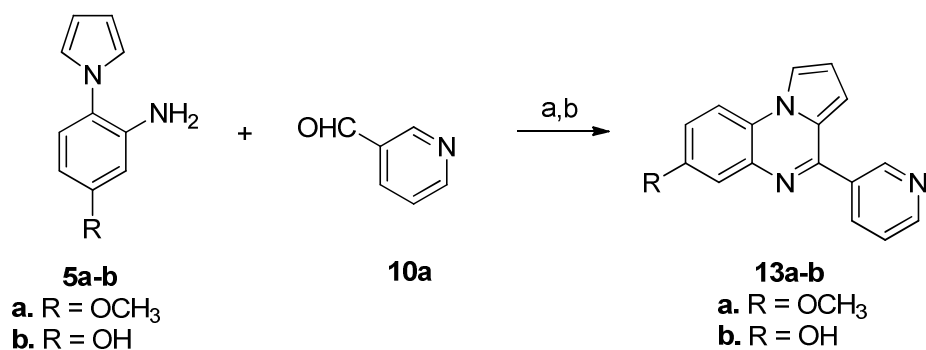
Scheme 6. Synthesis of Analogues 12a-m^a



27 Reagents and conditions: (a) 1,2,3-benzotriazole, AlCl₃, THF, overnight; (b) MnO₂, acetone, 55
28 °C, 24 h, 7-77% in two steps; (c) H₂, Pd/C, MeOH, 5 h, 50-93%.

32
33
34
35
36
37
38
39
40
41
42
43
44
45
46
47
48

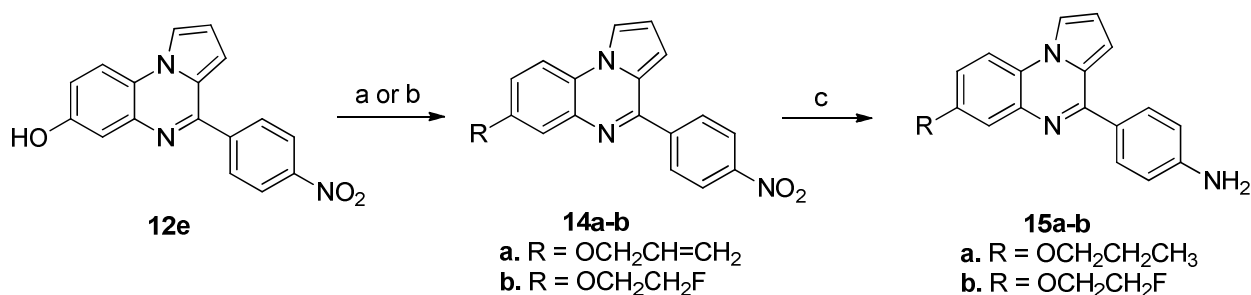
Scheme 7. Synthesis of Analogues 13a-b^a



49 Reagents and conditions: (a) 1,2,3-benzotriazole, AlCl₃, THF, overnight; (b) MnO₂, acetone, 55
50 °C, 24 h, 52-78% in two steps.

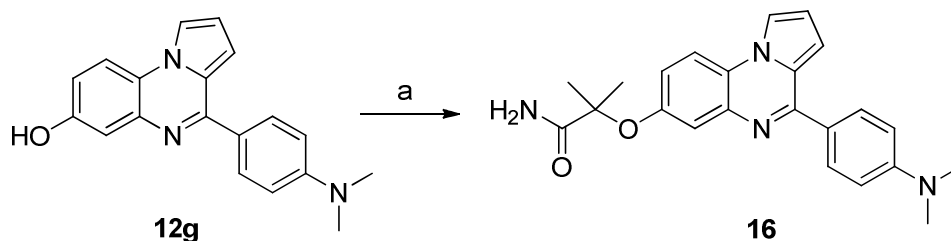
To explore the effects of replacing the hydroxyl group of compound **12f** with different alkyl groups, compound **12e** was first treated with allyl bromide to introduce the allyl group (**14a**), and then the nitro group was reduced by hydrogenation (in **Scheme 8**). The side chain double bond was also reduced under these conditions to afford the *n*-propoxy product **15a**. The fluoroethyl compound **15b** was prepared in a similar fashion but employed the Mitsunobu reaction to introduce the side chain (in **Scheme 8**).^{25, 26} An analogue **16** with a 2-methylpropionamide side chain was also prepared as shown in **Scheme 9**.

Scheme 8. Synthesis of Analogues 15a-b^a



Reagents and conditions: (a) allyl bromide, Cs₂CO₃, DMF, microwave, 80 °C, 30 min, 58%; (b) FCH₂CH₂OH, DEAD, Ph₃P, THF, microwave, 60 °C, 40 min; (c) H₂, Pd/C, MeOH, overnight, 36-45%.

Scheme 9. Synthesis of Analogues 16^a

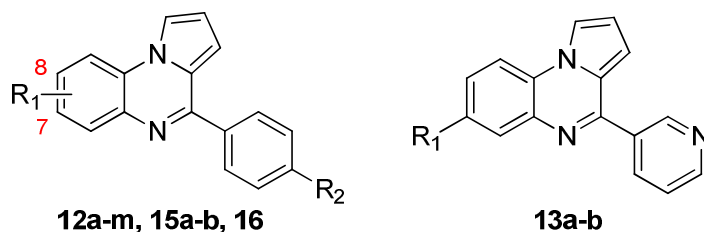


Reagents and conditions: (a) Br(CH₃)₂CHCONH₂, NaOH, DMA, 50 °C, 3 h, 41%.

The D-loop inhibitory activities for compounds **12a-m**, **13a-b**, **15a-b** and **16** are shown in **Table 3**. These results indicate that a methoxyl group in the 7 position of A-ring improves its D-loop inhibitory activity, which can be seen by comparing compound **12c** (IC_{50} 13.2 μ M) against **9g** (IC_{50} 22.1 μ M). A similar improvement was observed when a hydroxyl group was introduced at the same position (compare **12f**, IC_{50} 8.4 μ M and **12g**, IC_{50} 9.8 μ M against **9g**, IC_{50} 22.1 μ M and **9a**, IC_{50} 27.6 μ M). In contrast, the introduction of a fluorine atom in the 7 position or two fluorine atoms in the 7 and 8 positions of the A-ring yielded compounds whose D-loop inhibitory potential was moderately diminished (compound **12i** IC_{50} 25.0 μ M and **12l** IC_{50} 34.0 μ M) or nearly absent (compound **12j** and **12m**). For compounds with 3-pyridyl substituents (compound **13a** and **13b**), the incorporation of a methoxy or hydroxyl group in the A-ring yielded a slight improvement in D-loop inhibition compared with **11a**. The appendage of larger alkoxy groups at the 7 position of the A-ring (compounds **15a-b** and **16**) did not provide more potent D-loop inhibitors (except for compound **15b**), when compared to **9g**.

The influence of these alterations on RAD51-ssDNA binding activity was also evaluated for these analogs (**Table 3**). Most of the compounds influenced RAD51-ssDNA binding weakly or modestly, except for compounds **12b**, **15a**, **15b**, and **16**, which were stimulators of RAD51-ssDNA binding, and **12a**, which showed relatively strong ssDNA binding inhibition. Among the most potent D-loop inhibitors in this series, **12c** and **12g** only weakly influenced ssDNA-RAD51 binding; **12f** and **15b** exerted modest effects on ssDNA-RAD51 binding.

Table 3. The RAD51 D-loop inhibitory and RAD51-ssDNA binding stimulatory/inhibitory activities of **12a-m**, **13a-b**, **15a-b** and **16**.



Cpd	R ₁	R ₂	D-Loops		ssDNA binding	
			Max inhibition effect	IC ₅₀ (μM)	Max effect	IC ₅₀ (μM)
12a	7-OCH ₃	-OH	13±12%	>100	100±18%↓	35.0±14.0
12b	7-OCH ₃	-NO ₂	17±7%	>100	105±47%↑	Stim
12c	7-OCH ₃	-NH ₂	100±4%	13.2±2.8	29±8%↓	>100
12d	7-OH	-OH	97±8%	27.6±4.9	72±11%↓	>100
12e	7-OH	-NO ₂	13±10%	>100	92±21%↓	57.8±3.0
12f	7-OH	-NH ₂	100±3%	8.4±3.4	82±23%↓	96.9±44.9
12g	7-OH	-N(CH ₃) ₂	91±8%	9.8±3.5	34±32%↑	Stim
12i	7-F	-NH ₂	95±6%	25.0±5.1	60±18%↓	81.5±16.6
12j	7-F	-N(CH ₃) ₂	31±4%	>100	57±28%↑	Stim
12l	7,8-diF	-NH ₂	59±4%	34.0±2.9	42±8%↓	>100
12m	7,8-diF	-N(CH ₃) ₂	19±15%	>100	65±22%↑	Stim
13a	7-OCH ₃		74±5%	38.6±6.2	16±28%↓	>100
13b	7-OH		53±30%	64.9±31.6	87±10%↓	>100
15a		-NH ₂	75±7%	46.1±2.8	117±18%↑	Stim
15b		-NH ₂	98±5%	20.0±4.1	79±23%↑	Stim
16		-N(CH ₃) ₂	38±4%	>100	131±28%↑	Stim

“↑” Compound stimulates RAD51-ssDNA binding. “↓”Compound inhibits RAD51-ssDNA binding. “Stim” Compound is a stimulator.

Cellular effects of 1 and 9h. We used the DR-GFP assay to test the ability of select compounds to inhibit HR in human cells.²⁷ Briefly, cells containing the chromosomal DR-GFP reporter were transfected with a plasmid that expresses I-SceI, a rare-cutting endonuclease that makes a DSB within the DR-GFP cassette. Compounds were added at the time of transfection and the cells were outgrown for 24 hours. We noted that for longer outgrowth periods such as 48 hours, cells regained some HR activity (data not shown). This suggests the possibility of compensatory responses that oppose RAD51 inhibition by compounds; these effects will be detailed in a separate report. To overcome this technical limitation, we selected the relatively early time point of 24 hours to describe the in vivo effects of these compounds.

We demonstrated that **1** is able to inhibit HR activity in human cells (**Figure 5A**). Importantly, **1** yields 50% inhibition of cellular HR activity at 13.1 μM , which is comparable to its observed activity in biochemical assays. The HR inhibitory activity of **1** reaches 83% at concentrations of 40 μM , which is a dose where the RAD51-ssDNA binding activity remains unaffected in biochemical assays. Next, we compared **1** against its pure oxidized and pure reduced forms. In contrast to our results using biochemical assays, the inhibitory activity of **7** in the cell-based HR assay was comparable to that of **1** and **8**. As noted earlier, **7** spontaneously oxidizes to **8**. As such, this observed inhibitory activity of **7** is likely caused by its oxidation into the active constituent (**8**) during the HR assay; such would be expected given the relatively long (24-hour) incubation of **7** in an aerated tissue culture medium.

Next we used this cell-based HR quantification method to evaluate analogs that exhibited IC_{50} values less than 20 μM in biochemical D-loop assays. While compounds **12f** and **12g** had the lowest IC_{50} values in the D-loop assay, they both yielded comparable or slightly less inhibitory activity in the DR-GFP assay relative to **1** and **8**. The most potent inhibitor of cellular

HR was **9h**, having an IC_{50} of $3.0 \pm 1.8 \mu M$, which is over four-fold lower than the IC_{50} concentrations of the starting lead compound **1**.

Compound **9h** was tested further using cells containing the chromosomal DR-SSA reporter, which quantifies the ability of the cells to perform single-strand annealing (SSA), as a means to repair I-SceI induced DSBs. SSA is an alternative method of re-ligating DNA when HR cannot be completed. SSA efficiency is known to be elevated in situations where RAD51 function has been generally disrupted^{27,28}. Similarly, we previously demonstrated that both RI-1 and RI-2 induce elevated levels of SSA activity¹⁹. By contrast, we found that **9h** does not stimulate SSA, using a relevant concentration range that inhibits HR (**Figure 5b**). This suggests that **9h** stabilizes nucleoprotein filaments in a non-functional state, which are incapable of D-loop activity and simultaneously shielded from related (e.g. RAD52-mediated) pathways that promote SSA.

We tested whether **9h** permits the timely assembly of RAD51 into sub-nuclear foci in response to DNA damage. As expected, **9h** does not inhibit the appearance of RAD51 into sub-nuclear foci in response to radiation (**Figure 6a**), even at concentrations of **9h** that had inhibited cellular HR by 75% in prior DR-GFP assays (**Figure 5b**). Importantly, **9h** does not affect the co-localization of RAD51 foci with RPA, an HR associated protein that binds to ssDNA prior to the recruitment of RAD51 (**Figure 6b**). We observed 57% co-localization in **9h** treated cells and 60% co-localization in vehicle-treated cells. This important control confirms that our imaged sub-nuclear RAD51 puncta represent true DSB-associated foci, rather than off-target accumulations of RAD51 protein. Additionally, **9h** does not affect RAD51 protein levels (cytosolic, nuclear, or chromatin-bound fractions) at comparable time points (**Figure S3**). Our interpretation is further substantiated by quantitative gel-shift assays (**Figures 7a-c, S4**). We also

tested the selectivity of **9h** as a specific inhibitor of human RAD51 by comparing its ability to inhibit the D-loop activity of human RAD51 versus the distantly-related *S. cerevisiae* Rad51 and *E. coli* RecA recombinase proteins and found no significant inhibition of these proteins by **9h** (Figure 7d-f). Unlike the generalized RAD51 inhibitor RI-1, **9h** does not modulate the affinity of RAD51 to ssDNA or the stability of pre-formed RAD51-ssDNA complexes when challenged with high concentrations of salt.

Since **9h** inhibits HR-mediated repair of DSBs, we next investigated whether **9h** could sensitize cancer cells to radiation damage. Indeed, we observed that **9h** significantly sensitizes three different cancer cell lines, when **9h** was administered immediately after following irradiation and allowed to incubate with cells for the duration of clonogenic outgrowth thereafter (Figure 8). Given the substantial improvements of **9h** over the starting compound identified in our high throughput screen, we renamed compound **9h** as **RI(dl)-2**, for D-loop activity of RAD51 Inhibitor #2.

Conclusion

A common hallmark of tumor cells is the over-expression of the RAD51 recombinase protein. Numerous lines of evidence indicate that tumor cells are especially dependent upon the HR function of RAD51.^{11, 12, 29} This well-established feature of cancer cells has made RAD51 an attractive drug target, and several small molecules that inhibit cellular RAD51 function have been described as reviewed by Huang and Mazin¹⁶. In addition to its classical role in catalyzing homologous strand exchange, RAD51 additionally plays a central role in protecting stalled replication forks from nucleolytic degradation.^{21, 22} This protective function in replication requires that RAD51 is able to bind ssDNA, however it may not require the strand invasion

activity of RAD51. Therefore, we carried out a drug development campaign to inhibit RAD51's D-loop activity while sparing its ssDNA binding activity. Compound **1** was identified as a promising lead compound, and subsequent SAR efforts yielded compound **9h** with improved biochemical and cell-based activities.

We believe that this series of compounds represents a major step forward in the development of RAD51-targeting small molecules. To our current knowledge, these are the only known compounds that specifically inhibit RAD51's D-loop activity without interfering with its ability to bind ssDNA both in vitro and in cells. Halenaquinone was previously reported to strongly inhibit RAD51's D-loop activity while sparing its ssDNA binding activity in biochemical assays.²⁰ However, Halenaquinone was shown to inhibit the formation of RAD51 foci in human cells following irradiation, suggesting that in a cellular context this compound may prevent sufficient loading of RAD51 onto damaged DNA at the site of radiation-induced DSBs to form visible foci. Other characterized RAD51 inhibitors including our previously-described inhibitors RI-1 and RI-2 act by preventing RAD51 from loading onto damaged DNA.^{13,}

19

Compound **1** and its analogs represent potential cancer therapeutics aimed at sensitizing tumors to DNA-damaging therapies. Considering its high potency for inhibiting both D-loop formation and HR, compound **9h** provides an important candidate for further investigation. Meanwhile, since compound **9h** has almost no impact on RAD51-ssDNA binding, it also presents a novel tool for basic scientists who wish to study the different functions of RAD51.

Experimental Section

General. The nuclear magnetic resonance (^1H and ^{13}C NMR) spectra were obtained using a Bruker spectrometer with TMS as an internal standard. Automated column chromatography was performed using the CombiFlash Rf apparatus loaded with Merck silica gel (40–60 mesh). Preparative HPLC was carried out using a Shimadzu preparative liquid chromatograph with a column from ACE 5 AQ (150 mm \times 21.2 mm) with 5 μm particle size. All solvents used in preparative HPLC were spiked with 0.05% TFA. The purities of biologically important compounds are $\geq 95\%$ as determined by analytical HPLC (ACE 3AQ C18 column (150 mm \times 4.6 mm, particle size 3 μm), 0.05% TFA in H_2O /0.05% TFA in MeOH gradient eluting system).

General procedure for preparation of 4a-d. A solution of **2a-d** (20 mmol) and **3** (20 mmol) in acetic acid (30 mL) was heated to reflux for 3 h. After cooling down, the mixture was poured into water (150 mL) and extracted with diethyl ether (150 mL \times 3). The organic layers were combined and dried over Na_2SO_4 . Remove solvent provided the crude products of **4a-d**.

1-(4-Methoxy-2-nitrophenyl)-1H-pyrrole (4a).³⁰ The crude product of **4a** was further purified by flash silica gel column chromatography (ethyl acetate-hexanes, gradient up to 1:4) to provide the product as orange solid (90%). ^1H NMR (400 MHz, CDCl_3) δ 7.41-7.38 (m, 2 H), 7.19-7.16 (m, 1 H), 6.76 (s, 2 H), 6.35 (s, 2 H), 3.92 (s, 3 H); ^{13}C NMR (100 MHz, CDCl_3) δ 158.3, 145.6, 129.0, 126.9, 121.4, 118.8, 110.0, 109.1, 55.8.

3-Nitro-4-(1H-pyrrol-1-yl)phenol (4b).³¹ The crude product of **4b** was further purified by flash silica gel column chromatography (ethyl acetate-hexanes, gradient up to 1:2) to provide the product as orange solid (59%). ^1H NMR (400 MHz, methanol- d_4 and CDCl_3) δ 7.25-7.22 (m, 2 H), 7.05-7.02 (m, 1 H), 6.68 (s, 2 H), 6.25 (s, 2 H); ^{13}C NMR (100 MHz, methanol- d_4 and CDCl_3) δ 156.5, 145.6, 129.0, 125.6, 121.5, 119.8, 110.7, 109.5.

1-(4-Fluoro-2-nitrophenyl)-1*H*-pyrrole (4c). The crude product of **4c** was further purified by flash silica gel column chromatography (ethyl acetate-hexanes, gradient up to 1:7) to provide the product as yellow oil (63%). ¹H NMR (400 MHz, CDCl₃) δ 7.64-7.61 (m, 1 H), 7.52-7.48 (m, 1 H), 7.43-7.39 (m, 1 H), 6.80-6.78 (m, 2 H), 6.40-6.38 (m, 2 H).

1-(4,5-Difluoro-2-nitrophenyl)-1*H*-pyrrole (4d). The crude product of **4d** was further purified by flash silica gel column chromatography (ethyl acetate-hexanes, gradient up to 1:9) to provide the product as yellow oil (45%). ¹H NMR (400 MHz, CDCl₃) δ 7.85-7.80 (m, 1 H), 7.36-7.32 (m, 1 H), 6.78-6.76 (m, 2 H), 6.40-6.38 (m, 2 H).

General procedure for preparation of 5a-d. A suspension of **4a-d** (3 mmol) and palladium on charcoal (10%, 60 mg) in methanol (10 mL) was stirred under a hydrogen balloon for 5 h. The black solid was removed by filtration and the filtrate was concentrated to provide the crude product of **5a-d**.

5-Methoxy-2-(1*H*-pyrrol-1-yl)aniline (5a).³⁰ The crude product of **5a** was further purified by flash silica gel column chromatography (ethyl acetate-hexanes, gradient up to 1:4) to provide the product as pale yellow oil (97%). ¹H NMR (400 MHz, CDCl₃) δ 7.13-7.09 (m, 1 H), 6.83-6.82 (m, 2 H), 6.40-6.37 (m, 4 H), 3.84 (s, 3 H); ¹³C NMR (100 MHz, CDCl₃) δ 159.9, 143.4, 128.2, 122.1, 121.2, 109.2, 103.6, 101.1, 55.4.

3-Amino-4-(1*H*-pyrrol-1-yl)phenol (5b). The crude product of **5b** was further purified by flash silica gel column chromatography (ethyl acetate-hexanes, gradient up to 1:2) to provide the product as yellow solid (37%). ¹H NMR (400 MHz, methanol-*d*₄ and CDCl₃) δ 6.93-6.90 (m, 1 H), 6.71-6.69 (m, 2 H), 6.26-6.24 (m, 3 H), 6.22-6.19 (m, 1 H); ¹³C NMR (100 MHz, methanol-*d*₄ and CDCl₃) δ 156.7, 142.9, 127.8, 121.8, 120.1, 108.4, 105.1, 102.0.

5-Fluoro-2-(1*H*-pyrrol-1-yl)aniline (5c). The crude product of **5c** was further purified by flash silica gel column chromatography (ethyl acetate-hexanes, gradient up to 1:7) to provide the product as white solid (97%). ¹H NMR (400 MHz, CDCl₃) δ 7.16-7.12 (m, 1 H), 6.85-6.83 (m, 2 H), 6.55-6.50 (m, 2 H), 6.42-6.41 (m, 2 H).

4,5-Difluoro-2-(1*H*-pyrrol-1-yl)aniline (5d). The crude product **5d** was further purified by flash silica gel column chromatography (ethyl acetate-hexanes, gradient up to 1:7) to provide the product as white solid (87%). ¹H NMR (400 MHz, CDCl₃) δ 7.06-7.00 (m, 1 H), 6.82-6.80 (m, 2 H), 6.62-6.56 (m, 1 H), 6.39-6.38 (m, 2 H).

4-(7-Methoxy-4,5-dihydropyrrolo[1,2-*a*][13]quinoxalin-4-yl)-*N,N*-dimethylaniline (7). A mixture of the aniline **5a** (94 mg, 0.50 mmol), the benzaldehydes **6a** (75 mg, 0.50 mmol), 1,2,3-benzotriazole (59 mg, 0.50 mmol) and AlCl₃ (18 mg, 0.13 mmol) in THF (4 mL) was stirred at room temperature for 4 h. The mixture was diluted with water (15 mL) and extracted with ethyl acetate (15 mL X 3). The organic layers were combined, washed with saturated NaHSO₃ solutions (15 mL) three times, and then washed with 2 N NaOH aqueous solution (15 mL) and brine (15 mL) sequentially, dried over Na₂SO₄. The solvent was evaporated, the residue was further purified by flash silica gel column chromatography (ethyl acetate-hexanes, gradient up to 1:3). The purified product was recrystallized in methanol-acetonitrile (1:1, 3 mL) solutions to provide the pure product of **7** as white solid (52 mg, 32%). ¹H NMR (400 MHz, CDCl₃) δ 7.35-7.33 (m, 2 H), 7.27-7.24 (m, 1 H), 7.15-7.13 (m, 1 H), 6.76-6.73 (m, 2 H), 6.42-6.38 (m, 1 H), 6.31-6.30 (m, 1 H), 6.25-6.23 (m, 1 H), 5.62-5.60 (m, 1 H), 5.44 (s, 1 H), 4.11 (s, 1 H), 3.79 (s, 3 H), 2.98 (s, 6 H); ¹³C NMR (100 MHz, CDCl₃) δ 156.6, 150.2, 137.2, 129.8, 128.6, 128.4, 119.5, 115.0, 113.4, 112.0, 109.1, 104.8, 103.7, 100.8, 55.4, 55.0, 40.2; HRESIMS *m/z* calcd for

C₂₀H₂₂N₃O (MH⁺) 320.1763, found 320.1768. HPLC purity 98.3%, 98.9% (C-18 reverse phase, MeOH-H₂O).

General procedure for preparation of 8, 9a-j, 11a-d, 12a-m and 13a-b. A mixture of the aniline (**5a-d**, 1 mmol), the aldehyde (**6a-h** or **10a-d**, 1 mmol), 1,2,3-benzotriazole (1 mmol) and AlCl₃ (0.2 mmol) in THF (4 mL) was stirred at room temperature overnight. The mixture was diluted with water (15 mL) and extracted with ethyl acetate (15 mL X 3). The organic layers were combined, washed with 2 N NaOH solution (15 mL) and brine (15 mL) sequentially, and dried over Na₂SO₄ (for preparation of compounds with phenolic hydroxyl groups, including **9d**, **12a**, **12d-g** and **13b**, the organic layers were not washed with NaOH solution, only washed with brine). The solvent was evaporated, the residue was combined with MnO₂ (10 mmol) and dissolved with acetone (5 mL). The suspension was heated to 55 °C for 24 h. MnO₂ was removed by filtration, and the solvent was evaporated to provide the crude products of **8**, **9a-j**, **11a-d**, **12a-m** and **13a-b**.

4-(7-Methoxypyrrolo[1,2-a]quinoxalin-4-yl)-N,N-dimethylaniline (8). The aniline **5a** and benzaldehyde **6a** were reacted according to the general procedure, and the crude product was first purified by flash silica gel column chromatography (ethyl acetate-dichloromethane, gradient up to 3:17), and then further purified by preparative HPLC (with methanol-water, method 1) to afford the products **8** as TFA salt, orange solid (59%). ¹H NMR (400 MHz, methanol-*d*₄ and CDCl₃) δ 8.50-8.49 (m, 1 H), 8.06-8.03 (m, 1 H), 7.86-7.83 (m, 2 H), 7.57-7.55 (m, 1 H), 7.43-7.42 (m, 1 H), 7.21-7.16 (m, 2 H), 6.83-6.80 (m, 2 H), 3.88 (s, 3 H), 3.12 (s, 6 H); ¹³C NMR (100 MHz, methanol-*d*₄ and CDCl₃) δ 158.3, 153.7, 150.0, 131.0, 126.4, 122.2, 121.9, 119.2, 119.0, 117.9, 117.2, 116.0, 114.3, 111.4, 102.3, 55.2, 39.1; HRESIMS *m/z* calcd for C₂₀H₂₀N₃O (MH⁺) 318.1606, found 318.1598. HPLC purity 98.8%, 99.0% (C-18 reverse phase, MeOH-H₂O).

***N,N*-dimethyl-4-(pyrrolo[1,2-*a*]quinoxalin-4-yl)aniline (9a).** The aniline **5e** and benzaldehyde **6a** were reacted according to the general procedure, and the crude product was purified by flash silica gel column chromatography (ethyl acetate-dichloromethane, gradient up to 1:9) to provide the product **9a** as yellow solid (28%). ¹H NMR (400 MHz, methanol-*d*₄) δ 8.06-8.04 (m, 1 H), 7.89-7.87 (m, 1 H), 7.82-7.80 (m, 1 H), 7.76-7.73 (m, 2 H), 7.40-7.33 (m, 2 H), 6.94-6.92 (m, 1 H), 6.79-6.76 (m, 3 H), 2.96 (s, 6 H); ¹³C NMR (100 MHz, methanol-*d*₄) δ 154.4, 151.9, 135.4, 129.5, 127.9, 126.7, 126.6, 125.1, 124.8, 115.3, 113.7, 111.3, 109.4, 39.0; HRESIMS *m/z* calcd for C₁₉H₁₈N₃ (MH⁺) 288.1501, found 288.1506. HPLC purity 98.1%, 98.4% (C-18 reverse phase, MeOH-H₂O).

4-(3-Nitrophenyl)pyrrolo[1,2-*a*]quinoxaline (9b). The aniline **5e** and benzaldehyde **6b** were reacted according to the general procedure, and the crude product was purified by flash silica gel column chromatography (ethyl acetate-dichloromethane, gradient up to 1:19) to provide the product **9b** as light yellow solid (65%). ¹H NMR (400 MHz, CDCl₃) δ 8.93-8.91 (m, 1 H), 8.41-8.38 (m, 2 H), 8.07-8.04 (m, 2 H), 7.94-7.91 (m, 1 H), 7.76-7.72 (m, 1 H), 7.61-7.57 (m, 1 H), 7.53-7.49 (m, 1 H), 7.02-7.00 (m, 1 H), 6.98-6.95 (m, 1 H); ¹³C NMR (100 MHz, CDCl₃) δ 151.1, 148.1, 139.7, 135.5, 134.1, 130.0, 129.3, 127.9, 126.8, 125.2, 124.3, 124.1, 123.3, 114.8, 114.1, 113.4, 107.8; HRESIMS *m/z* calcd for C₁₇H₁₂N₃O₂ (MH⁺) 290.0930, found 290.0918. HPLC purity 99.5%, 99.4% (C-18 reverse phase, MeOH-H₂O).

4-(Pyrrolo[1,2-*a*]quinoxalin-4-yl)phenol (9d). The aniline **5e** and benzaldehyde **6c** were reacted according to the general procedure, and the crude product was first purified by flash silica gel column chromatography (ethyl acetate-dichloromethane, gradient up to 2:3), and then further purified by preparative HPLC (with methanol-water, method 1) to afford the products **9d** as TFA salt, yellow solid (57%). ¹H NMR (400 MHz, methanol-*d*₄) δ 8.87 (s, 1 H), 8.40-8.37 (m,

1 H), 8.03-8.01 (m, 1 H), 7.96-7.94 (m, 2 H), 7.82-7.78 (m, 1 H), 7.73-7.67 (m, 2 H), 7.35-7.33 (m, 1 H), 7.15-7.12 (m, 2 H); ^{13}C NMR (100 MHz, methanol- d_4) δ 163.0, 151.5, 131.6, 129.6, 127.3, 126.0, 125.8, 124.1, 123.1, 121.0, 120.3, 120.0, 118.6, 116.2, 115.5; HRESIMS m/z calcd for $\text{C}_{17}\text{H}_{13}\text{N}_2\text{O}$ (MH^+) 261.1028, found 261.1025. HPLC purity 99.5%, 99.5% (C-18 reverse phase, MeOH- H_2O).

4-(4-(Trifluoromethoxy)phenyl)pyrrolo[1,2-a]quinoxaline (9e). The aniline **5e** and benzaldehyde **6d** were reacted according to the general procedure, and the crude product was purified by flash silica gel column chromatography (ethyl acetate-hexanes, gradient up to 1:9) to provide the product **9e** as yellow solid (70%). ^1H NMR (400 MHz, CDCl_3) δ 8.08-8.03 (m, 3 H), 7.97 (s, 1 H), 7.85-7.82 (m, 1 H), 7.53-7.40 (m, 4 H), 6.97-6.96 (m, 1 H), 6.90-6.89 (m, 1 H); ^{13}C NMR (100 MHz, CDCl_3) δ 152.7, 150.3, 137.1, 136.1, 130.2, 130.1, 129.9, 127.7, 127.1, 125.3, 125.0, 124.4, 121.0, 120.5 (q, CF_3), 116.7, 114.8, 114.1, 113.6, 108.4; HRESIMS m/z calcd for $\text{C}_{18}\text{H}_{12}\text{N}_2\text{OF}_3$ (MH^+) 329.0902, found 329.0908. HPLC purity 97.3%, 97.1% (C-18 reverse phase, MeOH- H_2O).

4-(4-Nitrophenyl)pyrrolo[1,2-a]quinoxaline (9f).³² The aniline **5e** and benzaldehyde **6e** were reacted according to the general procedure, and the crude product was purified by flash silica gel column chromatography (ethyl acetate-dichloromethane, gradient up to 1:9) to provide the product **9f** as yellow solid (51%). ^1H NMR (400 MHz, CDCl_3) δ 8.43-8.40 (m, 2 H), 8.22-8.19 (m, 2 H), 8.07-8.05 (m, 2 H), 7.94-7.92 (m, 1 H), 7.62-7.57 (m, 1 H), 7.53-7.49 (m, 1 H), 6.97 (s, 2 H); ^{13}C NMR (100 MHz, CDCl_3) δ 151.4, 148.2, 144.0, 135.5, 130.1, 129.3, 128.0, 126.8, 125.3, 124.4, 123.4, 114.8, 114.1, 113.4, 107.9; HRESIMS m/z calcd for $\text{C}_{17}\text{H}_{12}\text{N}_3\text{O}_2$ (MH^+) 290.0930, found 290.0922. HPLC purity 99.0%, 98.1% (C-18 reverse phase, MeOH- H_2O).

***N*-ethyl-4-(pyrrolo[1,2-*a*]quinoxalin-4-yl)aniline (9h).** The aniline **5e** and benzaldehyde **6f** were reacted according to the general procedure, and the crude product was first purified by flash silica gel column chromatography (ethyl acetate-hexanes, gradient up to 1:3), and then further purified by preparative HPLC (with methanol-water, method 1) to afford the products **9h** as TFA salt, red oil (23%). ¹H NMR (400 MHz, methanol-*d*₄) δ 8.64 (s, 1 H), 8.19-8.16 (m, 1 H), 7.89-7.87 (m, 1 H), 7.80-7.78 (m, 2 H), 7.65-7.61 (m, 2 H), 7.56-7.52 (m, 1 H), 7.21-7.18 (m, 1 H), 6.80-6.77 (m, 2 H), 3.25 (q, *J* = 7.2 Hz, 2 H), 1.31 (t, *J* = 7.2 Hz, 3 H); ¹³C NMR (100 MHz, methanol-*d*₄) δ 154.1, 150.6, 131.6, 128.7, 127.0, 125.5, 125.3, 123.3, 122.4, 120.2, 119.9, 118.0, 115.2, 114.7, 112.0, 37.1, 13.0; HRESIMS *m/z* calcd for C₁₉H₁₈N₃ (MH⁺) 288.1501, found 288.1504. HPLC purity 98.5%, 98.4% (C-18 reverse phase, MeOH-H₂O).

4-(4-(Pyrrolidin-1-yl)phenyl)pyrrolo[1,2-*a*]quinoxaline (9i). The aniline **5e** and benzaldehyde **6g** were reacted according to the general procedure, and the crude product was first purified by flash silica gel column chromatography (ethyl acetate-hexanes, gradient up to 1:3), and then further purified by preparative HPLC (with methanol-water, method 1) to afford the products **9i** as TFA salt, orange solid (61%). ¹H NMR (400 MHz, methanol-*d*₄) δ 8.63 (s, 1 H), 8.17-8.14 (m, 1 H), 7.88-7.85 (m, 1 H), 7.77-7.74 (m, 2 H), 7.63-7.58 (m, 2 H), 7.54-7.50 (m, 1 H), 7.20-7.17 (m, 1 H), 6.60-6.58 (m, 2 H), 3.31 (s, 4 H), 2.07 (s, 4 H); ¹³C NMR (100 MHz, methanol-*d*₄) δ 151.7, 150.3, 131.4, 128.6, 127.0, 125.4, 125.2, 123.1, 122.3, 120.2, 119.9, 118.0, 115.1, 113.9, 111.7, 47.3, 24.9; HRESIMS *m/z* calcd for C₂₁H₂₀N₃ (MH⁺) 314.1657, found 314.1651. HPLC purity 95.6%, 97.7% (C-18 reverse phase, MeOH-H₂O).

4-(4-(Pyrrolo[1,2-*a*]quinoxalin-4-yl)phenyl)morpholine (9j). The aniline **5e** and benzaldehyde **6h** were reacted according to the general procedure. The crude product was combined with NaBH₄ (68mg, 1.8 mmol), dissolved with methanol (3 mL)-dichloromethane (0.5

mL) mixture solvent, and stirred at room temperature for 3 h. The mixture was diluted with water (10 mL) and extracted with ethyl acetate (10 mL X 3). The organic layers were combined and dried over Na₂SO₄. Solvent was evaporated and the residues were further purified by flash silica gel column chromatography (ethyl acetate-hexanes, gradient up to 1:2) and the product was recrystallized in acetonitrile to provide the product **9j** as yellow solid (19%). ¹H NMR (400 MHz, CDCl₃) δ 8.04-7.97 (m, 4 H), 7.87-7.84 (m, 1 H), 7.47-7.44 (m, 2 H), 7.06-7.04 (m, 3 H), 6.90-6.88 (m, 1 H), 3.92-3.87 (m, 4 H), 3.32-3.27 (m, 4 H); ¹³C NMR (100 MHz, CDCl₃) δ 153.5, 152.0, 136.1, 129.6, 129.4, 129.3, 126.6, 126.5, 125.0, 124.8, 114.5, 114.0, 113.4, 113.2, 108.1, 66.4, 48.3. HRESIMS *m/z* calcd for C₂₁H₂₀N₃O (MH⁺) 330.1606, found 330.1577. HPLC purity 98.4%, 98.9% (C-18 reverse phase, MeOH-H₂O).

4-(Pyridin-3-yl)pyrrolo[1,2-a]quinoxaline (11a). The aniline **5e** and aldehyde **10a** were reacted according to the general procedure and the crude product was purified by flash silica gel column chromatography (hexane-ethyl acetate, gradient up to 2:3) to provide the product **11a** as white solid (64%). ¹H NMR (400 MHz, CDCl₃) δ 9.26-9.25 (m, 1 H), 8.77-8.74 (m, 1 H), 8.31-8.29 (m, 1 H), 8.02-7.96 (m, 2 H), 7.84-7.81 (m, 1 H), 7.52-7.41 (m, 3 H), 6.96-6.94 (m, 1 H), 6.89-6.87 (m, 1 H); ¹³C NMR (100 MHz, CDCl₃) δ 150.9, 150.2, 149.0, 135.8, 135.6, 133.8, 129.8, 127.6, 126.7, 125.1, 124.5, 123.2, 114.7, 113.9, 113.3, 107.9. HRESIMS *m/z* calcd for C₁₆H₁₂N₃ (MH⁺) 246.1031, found 246.1038. HPLC purity 99.1%, 98.9% (C-18 reverse phase, MeOH-H₂O).

4-(Pyridin-4-yl)pyrrolo[1,2-a]quinoxaline (11b).³² The aniline **5e** and aldehyde **10b** were reacted according to the general procedure and the crude product was further purified by flash silica gel column chromatography (ethyl acetate-dichloromethane, gradient up to 7:3) to provide the product **11b** as yellow solid (64%). ¹H NMR (400 MHz, CDCl₃) δ 8.83-8.81 (m, 2

H), 8.05-8.02 (m, 2 H), 7.91-7.87 (m, 3 H), 7.58-7.54 (m, 1 H), 7.50-7.46 (m, 1 H), 7.00-6.98 (m, 1 H), 6.94-6.92 (m, 1 H); ^{13}C NMR (100 MHz, CDCl_3) δ 151.3, 149.9, 145.3, 135.5, 130.1, 127.9, 126.9, 125.1, 124.3, 122.5, 114.7, 114.0, 113.3, 107.8; HRESIMS m/z calcd for $\text{C}_{16}\text{H}_{12}\text{N}_3$ (MH^+) 246.1031, found 246.1025. HPLC purity 98.0%, 98.9% (C-18 reverse phase, MeOH- H_2O).

4-(Cyclohex-1-en-1-yl)pyrrolo[1,2-a]quinoxaline (11c).³³ The aniline **5e** and aldehyde **10c** were reacted according to the general procedure and the crude product was further purified by flash silica gel column chromatography (ethyl acetate-hexanes, gradient up to 1:9) to provide the product **11c** as pale yellow oil (35%). ^1H NMR (400 MHz, CDCl_3) δ 7.97-7.94 (m, 1 H), 7.92-7.91 (m, 1 H), 7.82-7.79 (m, 1 H), 7.48-7.40 (m, 2 H), 6.98-6.96 (m, 1 H), 6.85-6.83 (m, 1 H), 6.59-6.57 (m, 1 H), 2.69-2.67 (m, 2 H), 2.35-2.32 (m, 2 H), 1.90-1.86 (m, 2 H), 1.82-1.77 (m, 2 H); ^{13}C NMR (100 MHz, CDCl_3) δ 156.2, 136.3, 135.6, 130.8, 129.5, 126.7, 126.6, 124.8, 124.6, 113.8, 113.1, 113.0, 107.8, 26.6, 25.3, 22.4, 21.7; HRESIMS m/z calcd for $\text{C}_{17}\text{H}_{17}\text{N}_2$ (MH^+) 249.1392, found 249.1392. HPLC purity 98.8%, 98.9% (C-18 reverse phase, MeOH- H_2O).

4-(Naphthalen-1-yl)pyrrolo[1,2-a]quinoxaline (11d).³⁴ The aniline **5e** and aldehyde **10d** were reacted according to the general procedure and the crude product was first purified by flash silica gel column chromatography (ethyl acetate-hexanes, gradient up to 3:17), and then further purified by preparative HPLC (with methanol-water, method 0) to afford the products **11d** as TFA salt, pale yellow oil (71%). ^1H NMR (400 MHz, methanol- d_4 and CDCl_3) δ 8.50-8.49 (m, 1 H), 8.19-8.16 (m, 1 H), 8.13-8.11 (m, 2 H), 7.99-7.96 (m, 1 H), 7.84-7.82 (m, 1 H), 7.79-7.72 (m, 2 H), 7.67-7.61 (m, 2 H), 7.58-7.54 (m, 1 H), 7.48-7.44 (m, 1 H), 7.13-7.10 (m, 1 H), 7.03-7.02 (m, 1 H); ^{13}C NMR (100 MHz, methanol- d_4 and CDCl_3) δ 151.6, 133.3, 131.8, 130.4, 129.6,

128.3, 128.2, 128.1, 128.0, 127.2, 127.0, 126.5, 126.2, 124.8, 124.6, 124.1, 121.0, 117.5, 117.2, 114.6. HRESIMS m/z calcd for $C_{21}H_{15}N_2$ (MH^+) 295.1235, found 295.1228. HPLC purity 99.4%, 99.7% (C-18 reverse phase, MeOH-H₂O).

4-(7-Methoxypyrrolo[1,2-a]quinoxalin-4-yl)phenol (12a). The aniline **5a** and benzaldehyde **6c** were reacted according to the general procedure and the crude product was first purified by flash silica gel column chromatography (ethyl acetate-hexanes, gradient up to 2:3) and then further purified by preparative HPLC (with methanol-water, method 1) to afford the product **12a** as TFA salt, yellow solid (10 mg, 7%). ¹H NMR (400 MHz, methanol-*d*₄ and CDCl₃) δ 8.74-8.73 (m, 1 H), 8.49-8.48 (m, 1 H), 8.23-8.19 (m, 1 H), 8.15-8.12 (m, 1 H), 7.48-7.46 (m, 1 H), 7.44-7.41 (m, 1 H), 7.34-7.31 (m, 2 H), 7.17-7.15 (m, 1 H), 3.96 (s, 3 H). HRESIMS m/z calcd for $C_{18}H_{15}N_2O_2$ (MH^+) 291.1134, found 291.1144. HPLC purity 98.3%, 98.1% (C-18 reverse phase, MeOH-H₂O).

7-Methoxy-4-(4-nitrophenyl)pyrrolo[1,2-a]quinoxaline (12b). The aniline **5a** and benzaldehyde **6e** were reacted according to the general procedure and the crude product was further purified by flash silica gel column chromatography eluted with pure dichloromethane to provide the product **12b** as yellow solid (63%). ¹H NMR (400 MHz, CDCl₃) δ 8.41-8.38 (m, 2 H), 8.20-8.17 (m, 2 H), 7.99-7.98 (m, 1 H), 7.83-7.81 (m, 1 H), 7.51-7.50 (m, 1 H), 7.21-7.18 (m, 1 H), 6.94-6.91 (m, 2 H), 3.94 (s, 3 H); ¹³C NMR (100 MHz, CDCl₃) δ 157.0, 151.7, 148.2, 144.1, 136.6, 129.2, 124.2, 123.4, 121.1, 117.3, 114.4, 114.3, 113.8, 111.1, 107.5, 55.4; HRESIMS m/z calcd for $C_{18}H_{14}N_3O_3$ (MH^+) 320.1035, found 320.1020. HPLC purity 96.4%, 97.1% (C-18 reverse phase, MeOH-H₂O).

4-(4-Hydroxyphenyl)pyrrolo[1,2-a]quinoxalin-7-ol (12d). The aniline **5b** and benzaldehyde **6c** were reacted according to the general procedure and the crude product was

further purified by flash silica gel column chromatography (ethyl acetate-hexanes, gradient up to 3:2) to provide the product **12d** as yellow solid (40%). ¹H NMR (400 MHz, methanol-*d*₄) δ 8.14 (s, 1 H), 7.93-7.91 (m, 1 H), 7.80-7.77 (m, 2 H), 7.31-7.30 (m, 1 H), 7.06-7.03 (m, 1 H), 6.99-6.94 (m, 3 H), 6.87-6.85 (m, 1 H); ¹³C NMR (100 MHz, methanol-*d*₄) δ 158.9, 154.7, 154.3, 136.1, 129.5, 128.7, 124.2, 120.1, 115.6, 114.8, 114.5, 114.3, 113.0, 111.9, 108.6; HRESIMS *m/z* calcd for C₁₇H₁₃N₂O₂ (MH⁺) 277.0977, found 277.0983. HPLC purity 96.4%, 96.3% (C-18 reverse phase, MeOH-H₂O).

4-(4-Nitrophenyl)pyrrolo[1,2-a]quinoxalin-7-ol (12e). The aniline **5b** and benzaldehyde **6e** were reacted according to the general procedure and the crude product was first purified by flash silica gel column chromatography (ethyl acetate-dichloromethane, gradient up to 1:3), and then further purified by preparative HPLC (with methanol-water, method 1) to afford the products **12e** as TFA salt, yellow solid (49%). ¹H NMR (400 MHz, methanol-*d*₄ and CDCl₃) δ 8.50-8.47 (m, 2 H), 8.43 (s, 1 H), 8.17-8.14 (m, 2 H), 8.06-8.03 (m, 1 H), 7.42-7.41 (m, 1 H), 7.26-7.21 (m, 2 H), 7.14-7.13 (m, 1 H); HRESIMS *m/z* calcd for C₁₇H₁₂N₃O₃ (MH⁺) 306.0879, found 306.0876.. HPLC purity 99.4%, 99.5% (C-18 reverse phase, MeOH-H₂O).

4-(4-(Dimethylamino)phenyl)pyrrolo[1,2-a]quinoxalin-7-ol (12g). The aniline **5b** and benzaldehyde **6a** were reacted according to the general procedure and the crude product was first purified by flash silica gel column chromatography (ethyl acetate-dichloromethane, gradient up to 2:3) and then further purified by preparative HPLC (with methanol-water, method 1) to afford the products **12g** as TFA salt, orange solid (25%). ¹H NMR (400 MHz, methanol-*d*₄ and CDCl₃) δ 8.46 (s, 1 H), 8.01-7.99 (m, 1 H), 7.88-7.86 (m, 2 H), 7.59-7.57 (m, 1 H), 7.39-7.37 (m, 1 H), 7.19-7.17 (m, 2 H), 6.91-6.88 (m, 2 H), 3.16 (s, 6 H); ¹³C NMR (100 MHz, methanol-*d*₄ and CDCl₃) δ 156.6, 153.7, 150.2, 130.9, 126.5, 122.0, 121.9, 118.9, 118.5, 117.8, 116.0, 114.6,

111.5, 104.7, 39.2; HRESIMS m/z calcd for $C_{19}H_{18}N_3O$ (MH^+) 304.1450, found 304.1465.
HPLC purity 99.0%, 99.5% (C-18 reverse phase, MeOH-H₂O).

7-Fluoro-4-(4-nitrophenyl)pyrrolo[1,2-a]quinoxaline (12h). The aniline **5c** and benzaldehyde **6e** were reacted according to the general procedure and the crude product was further purified by flash silica gel column chromatography (ethyl acetate-dichloromethane, gradient up to 1:19) to provide the product **12h** as yellow solid (77%). ¹H NMR (400 MHz, CDCl₃) δ 8.44-8.42 (m, 2 H), 8.22-8.20 (m, 2 H), 8.05 (s, 1 H), 7.92-7.90 (m, 1 H), 7.76-7.73 (m, 1 H), 7.36-7.32 (m, 1 H), 7.00-6.98 (m, 2 H). HRESIMS m/z calcd for $C_{17}H_{11}N_3O_2F$ (MH^+) 308.0835, found 308.0837.

4-(7-Fluoropyrrolo[1,2-a]quinoxalin-4-yl)-N,N-dimethylaniline (12j). The aniline **5c** and benzaldehyde **6a** were reacted according to the general procedure and the crude product was purified by flash silica gel column chromatography (ethyl acetate-hexanes, gradient up to 1:2) to provide the product **12j** as yellow oil (77%). ¹H NMR (400 MHz, CDCl₃) δ 8.01-7.98 (m, 2 H), 7.91-7.89 (m, 1 H), 7.79-7.75 (m, 1 H), 7.71-7.67 (m, 1 H), 7.20-7.15 (m, 1 H), 7.10-7.08 (m, 1 H), 6.88-6.84 (m, 3 H), 3.07 (s, 6 H). HRESIMS m/z calcd for $C_{19}H_{17}N_3F$ (MH^+) 306.1406, found 306.1399. HPLC purity 96.4%, 97.4% (C-18 reverse phase, MeOH-H₂O).

7,8-Difluoro-4-(4-nitrophenyl)pyrrolo[1,2-a]quinoxaline (12k). The aniline **5d** and benzaldehyde **6e** were reacted according to the general procedure and the crude product was further purified by flash silica gel column chromatography (dichloromethane, 100%) to provide the product **12k** as yellow solid (41%). ¹H NMR (400 MHz, CDCl₃) δ 8.44-8.41 (m, 2 H), 8.20-8.18 (m, 2 H), 7.93-7.92 (m, 1 H), 7.89-7.84 (m, 1 H), 7.74-7.69 (m, 1 H), 7.01-6.99 (m, 2 H). HRESIMS m/z calcd for $C_{17}H_{10}N_3O_2F_2$ (MH^+) 326.0741, found 326.0738.

4-(7,8-Difluoropyrrolo[1,2-a]quinoxalin-4-yl)-N,N-dimethylaniline (12m). The aniline **5d** and benzaldehyde **6a** were reacted according to the general procedure and the crude product was purified by flash silica gel column chromatography (ethyl acetate-hexanes, gradient up to 1:2) to provide the product **12m** as yellow solid (50%). ¹H NMR (400 MHz, CDCl₃) δ 7.98-7.95 (m, 2 H), 7.81-7.76 (m, 2 H), 7.61-7.56 (m, 1 H), 7.09-7.07 (m, 1 H), 6.89-6.87 (m, 1 H), 6.85-6.83 (m, 2 H), 3.07 (s, 6 H). HRESIMS *m/z* calcd for C₁₉H₁₆N₃F₂ (MH⁺) 324.1312, found 324.1294. HPLC purity 97.3%, 97.2% (C-18 reverse phase, MeOH-H₂O).

7-Methoxy-4-(pyridin-3-yl)pyrrolo[1,2-a]quinoxaline (13a). The aniline **5a** and aldehyde **10a** were reacted according to the general procedure and the crude product was purified by flash silica gel column chromatography (ethyl acetate-hexanes, gradient up to 95:5) to afford the products **13a** as yellow solid (78%). ¹H NMR (400 MHz, methanol-*d*₄ and CDCl₃) δ 9.09-9.08 (m, 1 H), 8.69-8.67 (m, 1 H), 8.30-8.28 (m, 1 H), 7.97-7.96 (m, 1 H), 7.77-7.74 (m, 1 H), 7.56-7.52 (m, 1 H), 7.37-7.35 (m, 1 H), 7.09-7.05 (m, 1 H), 6.87-6.83 (m, 2 H), 3.86 (s, 3 H); ¹³C NMR (100 MHz, methanol-*d*₄ and CDCl₃) δ 156.9, 150.8, 149.6, 148.3, 136.4, 136.1, 133.9, 124.0, 123.5, 121.0, 116.7, 115.0, 114.4, 113.8, 110.3, 107.9, 54.9. HRESIMS *m/z* calcd for C₁₇H₁₄N₃O (MH⁺) 276.1137, found 276.1121. HPLC purity 99.4%, 98.7% (C-18 reverse phase, MeOH-H₂O).

4-(Pyridin-3-yl)pyrrolo[1,2-a]quinoxalin-7-ol (13b). The aniline **5b** and aldehyde **10a** were reacted according to the general procedure and the crude product was further purified by flash silica gel column chromatography (first eluted with ethyl acetate-hexanes 1:1, and then switched to methanol-dichloromethane 5:95), to afford the products **13b** as yellow solid (52%). ¹H NMR (400 MHz, methanol-*d*₄ and CDCl₃) δ 9.09-9.08 (s, 1 H), 8.70-8.68 (m, 1 H), 8.32-8.29 (m, 1 H), 8.04-8.03 (m, 1 H), 7.84-7.81 (m, 1 H), 7.59-7.55 (m, 1 H), 7.36-7.34 (m, 1 H), 7.13-

7.09 (m, 1 H), 6.90-6.88 (m, 2 H); ^{13}C NMR (100 MHz, methanol- d_4 and CDCl_3) δ 154.7, 150.9, 149.6, 148.3, 136.4, 136.2, 134.0, 124.1, 123.5, 120.5, 117.0, 115.0, 114.5, 113.7, 112.8, 108.1; HRESIMS m/z calcd for $\text{C}_{16}\text{H}_{12}\text{N}_3\text{O}$ (MH^+) 262.0980, found 262.0963. HPLC purity 97.0%, 97.0% (C-18 reverse phase, MeOH- H_2O).

General procedure for preparation of 9c, 9g, 12c, 12f, 12i and 12l. A suspension of the nitro compound **9b**, **9f**, **12b**, **12e**, **12h**, or **12k** (0.3 mmol) and palladium on charcoal (10%, 20 mg) in methanol (10 mL) was stirred under a hydrogen balloon for 5 h. The solid was removed and the filtrate was concentrated to provide the crude product of **9c**, **9g**, **12c**, **12f**, **12i**, and **12l**.

3-(Pyrrolo[1,2-a]quinoxalin-4-yl)aniline (9c). The compound **9b** was reduced by hydrogenation according the general procedure and the crude product was further purified by flash silica gel column chromatography (ethyl acetate-hexanes, gradient up to 3:2) to provide the product **9c** as pale yellow oil (57%). ^1H NMR (400 MHz, methanol- d_4) δ 8.14 (s, 1 H), 7.97-7.94 (m, 1 H), 7.86-7.84 (m, 1 H), 7.47-7.43 (m, 1 H), 7.40-7.35 (m, 1 H), 7.29-7.23 (m, 2 H), 7.18-7.15 (m, 1 H), 6.95-6.90 (m, 2 H), 6.85-6.83 (m, 1 H); ^{13}C NMR (100 MHz, methanol- d_4) δ 147.9, 138.5, 135.1, 128.9, 128.3, 127.4, 126.9, 124.9, 117.8, 116.6, 115.6, 114.9, 113.9, 113.8, 109.6; HRESIMS m/z calcd for $\text{C}_{17}\text{H}_{14}\text{N}_3$ (MH^+) 260.1188, found 260.1187. HPLC purity 99.6%, 98.8% (C-18 reverse phase, MeOH- H_2O).

4-(Pyrrolo[1,2-a]quinoxalin-4-yl)aniline (9g). The compound **9f** was reduced by hydrogenation according the general procedure and the crude product was purified by flash silica gel column chromatography (ethyl acetate-hexanes, gradient up to 3:2) to provide the product **9g** as yellow solid (87%). ^1H NMR (400 MHz, methanol- d_4 and CDCl_3) δ 8.03-8.02 (m, 1 H), 7.89-7.85 (m, 2 H), 7.74-7.69 (m, 2 H), 7.49-7.36 (m, 2 H), 7.02-7.00 (m, 1 H), 6.87-6.81 (m, 3 H); ^{13}C NMR (100 MHz, methanol- d_4 and CDCl_3) δ 154.1, 149.2, 134.5, 129.6, 127.5, 126.8, 126.4,

126.1, 125.0, 124.6, 115.3, 114.2, 113.9, 113.4, 109.9; HRESIMS m/z calcd for $C_{17}H_{14}N_3$ (MH^+) 260.1188, found 260.1170. HPLC purity 99.0%, 98.3% (C-18 reverse phase, MeOH- H_2O).

4-(7-Methoxypyrrolo[1,2-a]quinoxalin-4-yl)aniline (12c). The compound **12b** was reduced by hydrogenation according the general procedure and the crude product was further purified by flash silica gel column chromatography (ethyl acetate-hexanes, gradient up to 3:2) to provide the product **12c** as yellow oil (79%). 1H NMR (400 MHz, methanol- d_4) δ 7.87-7.86 (m, 1 H), 7.66-7.63 (m, 3 H), 7.22-7.21 (m, 1 H), 6.90-6.87 (m, 1 H), 6.85-6.80 (m, 2 H), 6.70-6.68 (m, 1 H), 3.78 (s, 3 H); ^{13}C NMR (100 MHz, methanol- d_4) δ 156.8, 154.3, 149.8, 135.8, 129.3, 126.0, 124.1, 120.5, 114.7, 114.6, 114.1, 113.7, 112.9, 109.1, 108.7, 54.2; HRESIMS m/z calcd for $C_{18}H_{16}N_3O$ (MH^+) 290.1293, found 290.1286. HPLC purity 98.7%, 99.5% (C-18 reverse phase, MeOH- H_2O).

4-(4-Aminophenyl)pyrrolo[1,2-a]quinoxalin-7-ol (12f). The compound **12e** was reduced by hydrogenation according the general procedure and the crude product was purified by preparative HPLC (with methanol-water, method 2) to afford the products **12f** as TFA salt, brown oil (50%). 1H NMR (400 MHz, methanol- d_4) δ 8.54-8.53 (m, 1 H), 8.05-8.02 (m, 1 H), 7.78-7.75 (m, 2 H), 7.57-7.56 (m, 1 H), 7.29-7.28 (m, 1 H), 7.17-7.15 (m, 1 H), 7.12-7.09 (m, 1 H), 6.93-6.90 (m, 2 H); ^{13}C NMR (100 MHz, methanol- d_4) δ 156.6, 153.5, 150.2, 131.1, 126.3, 122.4, 121.8, 118.7, 118.3, 117.4, 117.3, 116.0, 115.8, 113.9, 104.2; HRESIMS m/z calcd for $C_{17}H_{14}N_3O$ (MH^+) 276.1137, found 276.1146. HPLC purity 98.4%, 95.6% (C-18 reverse phase, MeOH- H_2O).

4-(7-Fluoropyrrolo[1,2-a]quinoxalin-4-yl)aniline (12i). The compound **12h** was reduced by hydrogenation according the general procedure and the crude product was first purified by flash silica gel column chromatography (ethyl acetate-hexanes, gradient up to 1:2), and then

further purified by preparative HPLC (with methanol-water, method 1) to afford the product **12i** as TFA salt, yellow solid (74%). ¹H NMR (400 MHz, methanol-*d*₄) δ 8.75-8.74 (m, 1 H), 8.38-8.34 (m, 1 H), 7.87-7.84 (m, 2 H), 7.73-7.68 (m, 2 H), 7.54-7.48 (m, 1 H), 7.28-7.26 (m, 1 H), 6.93-6.90 (m, 2 H). HRESIMS *m/z* calcd for C₁₇H₁₃N₃F (MH⁺) 278.1094, found 278.1099. HPLC purity 97.0%, 96.2% (C-18 reverse phase, MeOH-H₂O).

4-(7,8-Difluoropyrrolo[1,2-a]quinoxalin-4-yl)aniline (12l). The compound **12k** was reduced by hydrogenation according the general procedure and the crude product was further purified by flash silica gel column chromatography (ethyl acetate-hexanes, gradient up to 2:3) to provide the product **12l** as yellow solid (93%). ¹H NMR (400 MHz, methanol-*d*₄ and CDCl₃) δ 7.88-7.85 (m, 2 H), 7.82-7.77 (m, 2 H), 7.65-7.60 (m, 1 H), 7.06-7.05 (m, 1 H), 6.92-6.89 (m, 1 H), 6.84-6.81 (m, 2 H). HRESIMS *m/z* calcd for C₁₇H₁₂N₃F₂ (MH⁺) 296.0999, found 296.1003. HPLC purity 96.5%, 96.2% (C-18 reverse phase, MeOH-H₂O).

7-(Allyloxy)-4-(4-nitrophenyl)pyrrolo[1,2-a]quinoxaline (14a). A suspension of **12e** (86 mg, 0.282 mmol), allyl bromide (78 mg, 0.64 mmol) and cesium carbonate (136 mg, 0.42 mmol) in dry DMF (2 mL) was heated to 80 °C for 30 min in a microwave reactor under argon. After cooling down, the mixture was diluted with water (20 mL) and extracted with ethyl acetate (20 mL X 3). The organic layers were combined and dried over Na₂SO₄. The solvent was evaporated and the residues were further purified by flash silica gel column chromatography (ethyl acetate-hexanes, gradient up to 1:3) to afford the product **14a** as yellow solid (56 mg, 58%). ¹H NMR (400 MHz, CDCl₃) δ 8.41-8.38 (m, 2 H), 8.20-8.17 (m, 2 H), 7.98-7.97 (m, 1 H), 7.83-7.81 (m, 1 H), 7.51-7.50 (m, 1 H), 7.24-7.21 (m, 1 H), 6.94-6.91 (m, 2 H), 6.18-6.08 (m, 1 H), 5.52-5.47 (m, 1 H), 5.37-5.33 (m, 1 H), 4.68-4.66 (m, 2 H); ¹³C NMR (100 MHz, CDCl₃) δ 156.0, 151.7,

1
2
3 148.2, 144.1, 136.6, 132.4, 129.2, 124.2, 123.4, 121.2, 117.8, 117.7, 114.4, 114.3, 113.8, 112.2,
4
5 107.5, 68.9. HRESIMS m/z calcd for $C_{20}H_{16}N_3O_3$ (MH^+) 346.1192, found 346.1162.
6
7

8 **4-(7-Propoxypyrrolo[1,2-a]quinoxalin-4-yl)aniline (15a).** A suspension of **14a** (56 mg,
9 0.162 mmol) and palladium on charcoal (10%, 18 mg) in methanol (5 mL) was stirred under a
10 hydrogen balloon overnight. The solid was removed and the filtrate was concentrated. The
11 residue was further purified by flash silica gel column chromatography (ethyl acetate-hexanes,
12 gradient up to 3:2) to provide the product **15a** as yellow oil (23 mg, 45%). 1H NMR (400 MHz,
13 methanol- d_4) δ 8.07-8.06 (m, 1 H), 7.86-7.84 (m, 1 H), 7.71-7.68 (m, 2 H), 7.30-7.29 (m, 1 H),
14 7.05-7.02 (m, 1 H), 6.96-6.95 (m, 1 H), 6.87-6.82 (m, 3 H), 4.00-3.96 (m, 2 H), 1.85-1.80 (m, 2
15 H), 1.09-1.05 (m, 3 H); ^{13}C NMR (100 MHz, methanol- d_4) δ 156.4, 154.4, 149.9, 135.6, 129.3,
16 125.8, 124.1, 120.5, 115.4, 115.0, 114.3, 113.8, 113.2, 109.8, 109.1, 69.3, 21.8, 9.1. HRESIMS
17 m/z calcd for $C_{20}H_{20}N_3O$ (MH^+) 318.1606, found 318.1588. HPLC purity 97.7%, 98.2% (C-18
18 reverse phase, MeOH- H_2O).
19
20
21
22
23
24
25
26
27
28
29
30
31
32
33

34 **4-(7-(2-Fluoroethoxy)pyrrolo[1,2-a]quinoxalin-4-yl)aniline (15b).** A solution of **12e** (69
35 mg, 0.226 mmol), 2-fluoroethanol (89 mg, 1.4 mmol) and triphenylphosphine (183 mg, 0.70
36 mmol) in dry THF (4 mL) was stirred under argon and cooled to 0 °C. DEAD (145 mg, 0.83
37 mmol) was added dropwise. The mixture was warmed to room temperature and heated to 60 °C
38 for 40 min in a microwave reactor. The solvent was evaporated and the residues were further
39 purified by flash silica gel column chromatography (ethyl acetate-hexanes, gradient up to 3:7) to
40 provide the crude product **14b**. The crude product **14b** was dissolved in methanol (5 mL), and
41 palladium on charcoal (10%, 29 mg) was added. The suspension was stirred under a hydrogen
42 balloon overnight. The solid was removed and the filtrate was concentrated. The residue was
43 further purified by flash silica gel column chromatography (ethyl acetate-hexanes, gradient up to
44
45
46
47
48
49
50
51
52
53
54
55
56
57
58
59
60

2:1) to provide the product **15b** as yellow oil (26 mg, 36%). ¹H NMR (400 MHz, methanol-*d*₄) δ 8.02-8.00 (m, 1 H), 7.82-7.79 (m, 1 H), 7.69-7.67 (m, 2 H), 7.29-7.28 (m, 1 H), 7.05-7.01 (m, 1 H), 6.94-6.92 (m, 1 H), 6.85-6.82 (m, 2 H), 6.81-6.78 (m, 1 H), 4.82-4.80 (m, 1 H), 4.70-4.68 (m, 1 H), 4.29-4.27 (m, 1 H), 4.22-4.20 (m, 1 H); ¹³C NMR (100 MHz, methanol-*d*₄) δ 155.7, 154.4, 150.0, 135.6, 129.4, 125.7, 124.1, 120.9, 115.2, 115.0, 114.4, 113.7, 113.2, 109.9, 109.1, 82.2, 80.5, 67.3, 67.1. HRESIMS *m/z* calcd for C₁₉H₁₇N₃OF (MH⁺) 322.1356, found 322.1330. HPLC purity 97.6%, 97.7% (C-18 reverse phase, MeOH-H₂O).

2-((4-(4-(Dimethylamino)phenyl)pyrrolo[1,2-a]quinoxalin-7-yl)oxy)-2-methylpropanamide (16). A solution of **12g** (84 mg, 0.28 mmol), NaOH (180 mg, 4.5 mmol) in DMA (3 mL) was stirred at room temperature for 1 h, 2-bromo-2-methylpropanamide (131 mg, 0.789 mmol) was added and the mixture was heated to 50 °C for 3 h. After cooling down, the mixture was diluted with water (12 mL), extracted with ethyl acetate (20 mL X 3). The organic layers were combined, washed with brine (20 mL) and dried over Na₂SO₄. The solvent was evaporated and the residues were further purified by flash silica gel column chromatography (ethyl acetate-hexanes, gradient up to 19:1) and the crude product was further purified by preparative HPLC (with methanol-water, method 1) to afford the product **16** as TFA salt, yellow solid (55 mg, 41%). ¹H NMR (400 MHz, methanol-*d*₄) δ 8.63-8.62 (m, 1 H), 8.20-8.17 (m, 1 H), 7.91-7.88 (m, 2 H), 7.67-7.65 (m, 1 H), 7.54-7.53 (m, 1 H), 7.36-7.32 (m, 1 H), 7.24-7.22 (m, 1 H), 6.94-6.91 (m, 2 H), 3.14 (s, 6 H), 1.65 (s, 6 H); ¹³C NMR (100 MHz, methanol-*d*₄) δ 177.3, 153.9, 153.5, 150.3, 131.0, 125.9, 122.8, 122.0, 121.5, 120.5, 119.3, 117.8, 115.9, 114.3, 111.3, 109.6, 81.2, 38.4, 23.8. HRESIMS *m/z* calcd for C₂₃H₂₅N₄O₂ (MH⁺) 389.1978, found 389.1956. HPLC purity 98.6%, 97.1% (C-18 reverse phase, MeOH-H₂O).

Cells, media, plasmids, and proteins.

The 293-DR-GFP and 293-SA-GFP reporter cell lines along with the pBASce I-SceI expressing and pCAGGS empty vector control plasmids were kindly provided by Jeremy Stark and described previously.²⁷ All cell lines except for PC-3 were maintained in complete DMEM (DMEM + 4.5 g/L D-glucose + L-glutamine + 10% fetal calf serum + penicillin/streptomycin); PC-3 cells were maintained in DMEM:F12 (1:1) with 10% fetal calf serum and penicillin/streptomycin. Human RAD51 protein was purified as described previously²³ and the purity was confirmed by SDS-PAGE (**Figure S5**). Rad51 and Rad52 proteins from *Saccharomyces cerevisiae* were kindly provided by Yuen-Ling Chan and purified as described previously³⁵. RecA protein from *Escherichia coli* was purchased from New England Biolabs.

Screening libraries.

We conducted high-throughput screening of the ASDI Diversity library of 6800 compounds and the Library of Pharmacologically Active Compounds (LOPAC1280). From each of the library master plates, 2.5 nmol of compound was acoustically transferred to individual assay plates at Nextval, Inc. This gave a final concentration of 50 μ M for each library compound in 50 μ l per well of final reaction volume for both the RAD51-DNA binding and RAD51-mediated strand pairing assays.

Fluorescence polarization-based RAD51-DNA binding assay.

The fluorescence polarization-based DNA binding assay was performed as previously described with a few modifications.²³ Reactions were carried out in black 384-well polystyrene plates. In each well, RAD51 protein was combined with reaction buffer and varying concentrations of

compound in DMSO in an initial volume of 40 μ l and incubated at 37 $^{\circ}$ C for 40 minutes. Then, 10 μ l of reaction buffer containing fluorescently-labeled ssDNA substrate (5'-Alexa488-oligo-dT₄₅) was added and the reaction incubated at 37 $^{\circ}$ C for another 40 minutes, after which the plate was read on a Tecan Infinite 200 Pro plate reader equipped with two sets of 485 \pm 25 nm / 535 \pm 35 nm with parallel or perpendicularly-oriented polarization filters. In both steps of the reaction setup, buffer components were maintained at 20 mM HEPES-NaOH (pH 7.5), 2 mM ATP, 10 mM MgCl₂, 0.1 mM TCEP-HCl (tris(2-carboxyethyl)phosphine), and 0.25 μ M BSA. The final reaction contained 4% DMSO, 0.2 μ M RAD51, 30 mM NaCl, 2% glycerol, and 2.22 nM ssDNA substrate. Compound IC₅₀ values were obtained by least-squares regression fitting of appropriate linear, log, or sigmoid dose-response models to the data, with the standard error indicated.

Solution assay for RAD51-mediated strand pairing.

The FRET-based solution assay for RAD51-mediated strand pairing was performed as described previously using the 51-nt Black Hole Quencher (BHQ1)-tagged ssDNA substrate DHD-HQ and the 162-bp Alexa488-tagged dsDNA substrate DHD162²⁴. Reactions were performed in black 384-well polystyrene plates. RAD51 in reaction buffer and compound in DMSO were combined in 20 μ l and incubated at room temperature for 40 minutes. Then, 10 μ l of solution containing the ssDNA substrate and CaCl₂ was added to each well and the reaction was incubated at 37 $^{\circ}$ C for 5 minutes to allow RAD51-ssDNA filaments to form. Finally, 20 μ l of solution was added containing the dsDNA double hairpin substrate with homology to the ssDNA substrate and the plate was incubated at 37 $^{\circ}$ C for 50 minutes to allow RAD51-mediated strand invasion, which is measured as a decrease in fluorescence intensity as the BHQ1-tagged ssDNA is paired with the Alexa488-tagged dsDNA. The final reaction contained 25 mM HEPES-NaOH (pH 7.5), 3 mM

ATP, 1 mM TCEP-HCl, 1.5 μ M BSA, 4% DMSO, 0.1 μ M RAD51, 2 mM NaCl, 0.1% glycerol, 10 nM ssDNA, and 5 nM dsDNA. The concentration of CaCl_2 was maintained at 5 mM throughout all three steps of the reaction setup. Fluorescence measurements were taken on a Tecan Infinite 200 Pro plate reader equipped with 485 ± 20 nm / 535 ± 35 nm filters.

Gel-based RAD51-DNA binding assays.

Human RAD51 protein in reaction buffer was combined with compound in DMSO in a total volume of 9 μ l, incubated at 37 $^\circ\text{C}$ for 40 minutes, and then 1 μ l of 4,373-nt closed circular pRS306 virion ssDNA was added and the reaction was incubated at 37 $^\circ\text{C}$ for an additional 5 minutes. At this point, the reaction consisted of 25 mM HEPES-NaOH (pH 7.0), 3 mM ATP, 5 mM MgCl_2 , 1 mM TCEP, 100 $\mu\text{g/ml}$ BSA, 0.5 μ M RAD51, and 1.5 μ M nucleotide concentration ssDNA. For experiments to determine the stability of RAD51-ssDNA complexes in salt, 1 μ l of NaCl was added to achieve the indicated concentration and the reaction was incubated for an additional 5 minutes at 37 $^\circ\text{C}$. RAD51-ssDNA complexes were fixed by addition of glutaraldehyde in 2 μ l to 0.25%, incubated for 5 minutes at 37 $^\circ\text{C}$, and run on a 1% agarose / 1X TAE gel, which was stained in SYBR Gold (Molecular Probes) and photographed under UV light.

Gel-based D-loop assay.

Recombinase protein in reaction buffer was combined with compound in DMSO in a total volume of 8 μ l, incubated at 37 $^\circ\text{C}$ for 10 minutes, and then 1 μ l of 5'- ^{32}P -labeled 90-mer ssDNA (5'-TACGAATGCACACGGTGTGGTGGGCCAGGTATTGTTAGCGGTTTGAAGCAGGC GGCAGAAGAAGTAACAAAGGAACCTAGAGGCCTTTT) with homology to the plasmid

pRS306³⁶ was added and the reaction was incubated at 37 °C for an additional 5 minutes. Then 1 µl of supercoiled pRS306 dsDNA plasmid was added to the reaction and incubated at 37 °C for 20 minutes. At this point, reactions containing human RAD51 protein consisted of 25 mM HEPES-NaOH (pH 7.0), 1 mM ATP, 1 mM MgCl₂, 1 mM DTT, 1.5 µM BSA, 4.5% DMSO, 0.5 µM RAD51, 11 mM NaCl, 1% glycerol, 20 nM ssDNA, and 5 nM pRS306 dsDNA. For reactions containing *Saccharomyces cerevisiae* Rad51 + Rad52 proteins or *Escherichia coli* RecA protein, the reactions were carried out in a manner similar to the one described for the human proteins, except MgCl₂ was present at 1 mM during the incubation with ssDNA and then increased to 10 mM during the incubation with dsDNA; the reaction buffer during incubation with dsDNA consisted of 20 mM HEPES-NaOH (pH 7.5), 2 mM ATP, 10 mM MgCl₂, 1 mM DTT, 100 µg/ml BSA 10 nM ssDNA, and 4.5 nM dsDNA. HsRAD51 was present at 0.5 to 1.5 µM depending on the specific D-loop activity of the protein prep, ScRad51 and ScRad52 were both present at 1 µM and 2 µM respectively, and EcRecA was present at 0.4 µM. The reactions were de-proteinized with 0.8% SDS and 0.8 mg/ml proteinase K, mixed with gel loading buffer, and run on a 0.9% agarose / 1X TAE gel. The gel was dried under vacuum on a positively-charged nylon membrane for 2 hours at 80 °C, exposed to a phosphor screen overnight, and imaged on a Storm 860 PhosphorImager. Quantitation of free oligo and D-loop bands was performed using ImageJ software (NIH, Bethesda, MD) and compound IC₅₀ values were obtained by least-squares regression fitting of appropriate linear, log, or sigmoid dose-response models to the data, with the standard error indicated.

Detection of RAD51 protein in subcellular fractions.

Subconfluent dishes of 293-DR-GFP cells were grown in the presence of compound for the indicated times, washed once with ice-cold PBS, and processed for subcellular fractionation at 4 °C. Soluble nuclear fractions were obtained by incubating cells in 5 pellet volumes of hypotonic buffer (10 mM HEPES-NaOH (pH 7.9), 10 mM KCl, 1.5 mM MgCl₂, 1 mM DTT, 10 mM NaF, 2 mM sodium orthovanadate, 2 mM sodium pyrophosphate, Complete Mini protease inhibitors (Roche)) on ice for 15 minutes, pelleting the cells, and saving the supernatant as the cytosolic fraction. The pellet was then resuspended in 1.5 pellet volumes of hypotonic buffer + 0.5 M NaCl, incubated on ice for 15 minutes, and the supernatant containing the soluble nuclear fraction was saved. Chromatin fractions were obtained from cells by extracting three times for 5 minutes each at 4 °C in 5 pellet volumes of RIPA buffer (50 mM Tris-HCl (pH 8.0), 150 mM NaCl, 1% Triton X-100, 0.5% sodium deoxycholate, 0.1% SDS, 10 mM NaF, 1 mM sodium orthovanadate, 2 mM sodium pyrophosphate, Complete Mini protease inhibitors (Roche)) to remove total soluble proteins and saving the pellet containing the insoluble chromatin fraction. Samples of subcellular fractions were boiled for 5 minutes in SDS-PAGE loading buffer (25 mM Tris-HCl (pH 6.8), 1% SDS, 2.5 % β-mercaptoethanol, 5 mM DTT, 0.0015% bromophenol blue, 5% glycerol), separated on a 10% SDS-PAGE, and transferred to a PVDF membrane by overnight electrophoretic transfer. The membrane was probed with primary antibody (rabbit anti-human RAD51 polyclonal antibody from Pacific Immunology at a 1:2000 dilution, or rabbit anti-human PCNA polyclonal antibody from Millipore at a 1:1000 dilution) followed by secondary antibody (HRP-conjugated donkey anti-rabbit IgG from GE Healthcare at a 1:2000 dilution) and developed with Western Lightning Plus-ECL reagent (Perkin-Elmer).

Quantitation of DNA repair efficiency in cells.

293-DR-GFP or 293-SA-GFP cells were electroporated in Opti-MEM with 37.5 $\mu\text{g/ml}$ of the I-Sce-I endonuclease bearing pCBASce plasmid or the pCAGGS empty vector control in 0.4 cm cuvettes at 325 V, 975 μF and seeded into 6-well plates with 2.5 ml complete DMEM + 0.5% DMSO with compound and allowed to outgrow for 24 hours. Following outgrowth, cells were harvested and suspended in PBS with 1 $\mu\text{g/ml}$ 7-aminoactinomycin D (7-AAD) and analyzed on a BD FACSCalibur flow cytometer. Dead and apoptotic cells were gated out based on size, shape, and 7-AAD staining. The fraction of GFP-positive cells was determined within the population of live cells.

Clonogenic survival assay.

Cells were grown in flasks to subconfluence, irradiated with X-rays at 1.5 Gy/min using a Philips RT250 Maxitron, trypsinized, and seeded at 1,000 to 1,500 cells per well in 6-well cluster plates (Corning 3516) in complete media with 0.5% DMSO and the indicated dose of compound. The plates were incubated for 7 to 11 days, until colonies of at least 50 cells formed, washed once with PBS, fixed and stained for at least 30 minutes at room temperature in 6% glutaraldehyde + 0.5% crystal violet, washed twice in cold tap water, dried, photographed, and scored using a custom macro set in ImageJ for automatic colony counting.

RAD51 cytological focus formation.

Cells were grown on glass coverslips for two days prior to irradiation with X-rays at 1.5 Gy/min using a Philips RT250 Maxitron. Following the indicated outgrowth time of 0, 2, 4, or 8 hours, coverslips to be co-stained with RAD51 and RPA were washed once in PBS, fixed in ice-cold fixative solution (3% paraformaldehyde, 3.4% sucrose in 1X PBS) for 10 minutes at room

temperature, washed three times in PBS, incubated in permeabilization buffer (20 mM HEPES-NaOH (pH 7.4), 50 mM NaCl, 3 mM MgCl₂, 0.5% Triton X-100, 300 mM sucrose) for 10 minutes at room temperature, washed three times in PBS, and incubated for at least 15 minutes in blocking buffer (1% BSA in 1X PBS) at 4 °C. For coverslips to be co-stained with RAD51 and γ H2AX, the same procedure was carried out with the fixation and permeabilization steps reversed. The coverslips were incubated with primary antibody (rabbit anti-human RAD51 polyclonal antibody from Pacific Immunology, mouse anti- γ H2AX monoclonal antibody clone JBW301 from Millipore, or mouse anti-RPA monoclonal antibody clone RPA34-19 from Calbiochem) at a 1:1000 dilution in blocking buffer for 18 hours at 4 °C, washed 3 times in PBS, incubated with secondary antibody (Alexa488-conjugated goat anti-rabbit IgG polyclonal antibody from Invitrogen, or Alexa594-conjugated goat anti-mouse IgG polyclonal antibody from Invitrogen) at a 1:1000 dilution in blocking buffer for 1 hour at room temperature, washed 3 times in PBS, air-dried, and mounted onto glass slides in Vectashield with DAPI H-1200 (Vector laboratories). Slides were viewed on a Zeiss Axio Imager.M1 epifluorescence microscope equipped with a CCD camera for acquiring images of at least 100 randomly-selected nuclei per test condition at a representative focal plane within the nuclear volume. Sub-nuclear RAD51, RPA, and γ H2AX foci were quantified using ImageJ using a custom macro set that automatically counts foci. Focus co-localization was scored for overlapping RAD51 and RPA foci in nuclei that contained at least 5 RPA foci and for RAD51 and γ H2AX foci in nuclei that contained at least 5 γ H2AX foci and did not exhibit pan-nuclear γ H2AX staining. Plots of RAD51 foci were generated using R software with the optional Bee Swarm package.^{37, 38}

Supporting Information

The supporting information is available free of charge on the ACS Publication website.

NMR spectrum of compound 1, 7 and 8, Mass spectrum of compound 1, representative D-loop gel images used to generate D-loop IC₅₀ values in Tables 1-3, RAD51 protein levels in cytosolic, soluble nuclear, and chromatin subcellular fractions of cells treated with or without **9h**, representative gel images of salt-titration midpoint experiments from Figure 7e, coomassie-stained SDS-PAGE of the human RAD51 preparation used for D-loop and DNA binding assays (PDF).

SMILES molecular formula strings (CSV).

AUTHOR INFORMATION

Corresponding Author

Alan P. Kozikowski, Phone: +1 312-996-7577. E-mail: kozikowa@uic.edu

Philip P. Connell, Phone: +1 773-834-8119. E-mail: pconnell@radonc.uchicago.edu

Author Contributions

[§]W.L. and B.B. contributed equally and are considered as co-first authors.

[¶]P.P.C and A.P.K contributed equally and are considered as co-last authors.

Notes

The authors declare no competing financial interest.

ACKNOWLEDGMENT

We thank Yuen-Ling Chan for providing recombinase proteins and DNA substrates used in the D-loop gel assay and gel shift assays. This work was funded by NIH grants 2R01CA142642 to P.P.C and A.P.K, as well as funding from the Wendy Will Cancer Fund.

ABBREVIATIONS USED

HR, homologous recombination; DSBs, DNA double strand breaks; ICLs, interstrand cross-links; ssDNA, single-stranded DNA; NHEJ, non-homologous end-joining; SAR, structure activity relationship; HT, high-throughput.

Figure Legends:

Figure 1. Schematic representation of the mechanism of DNA double strand breaks repair by homologous recombination. Following a DSB, the DNA ends are resected to generate 3' ssDNA overhangs onto which RAD51 loads. The resulting RAD51-ssDNA nucleoprotein filament is capable of invading homologous dsDNA and base-pairing with complementary DNA, thereby forming a heteroduplex and displacing a loop (D-loop) of ssDNA.

Figure 2. High-throughput (HT) screen for compounds that inhibit RAD51's D-loop activity: **A)** One biochemical assay monitors RAD51 binding to fluorescently-labeled ssDNA, which is detected as an increase in fluorescence polarization. **B)** A second parallel biochemical assay monitors fluorescence intensity, which decreases upon pairing of Black Hole Quencher 1-labeled ssDNA with a fluorescein-labeled complementary double-hairpin duplex. **C)** Compounds were tested for the ability to influence the efficiency of these two RAD51-mediated processes, and the results of this HT are displayed. Blue symbols = ASDI library compounds, red symbols = LOPAC library compounds. Arrow indicates the position of compound **1**.

Figure 3. Compound **1** inhibits RAD51's D-loop activity with minimal interference of RAD51-ssDNA binding. **A)** Electromobility shift assay showing that **1** does not inhibit interaction with RAD51 and ssDNA. **B)** Gel-based D-loop formation assay showing that **1** inhibits RAD51-mediated assimilation of a radiolabeled ssDNA oligonucleotide into the homologous region of a supercoiled dsDNA plasmid by up to 74%. Error bars indicate the standard error for four replicates with a representative gel image shown.

Figure 4. An overview is shown for the optimization strategy of **8**.

Figure 5. A) Inhibition of cellular HR activity by **1** and optimized analogs of **1** using the DR-GFP assay. Data were collected at 24 hours following transfection with the I-SceI expressing plasmid pCBASce. Error bars denote the standard error for three replicates. **B)** Inhibition of cellular HR and SSA activity by **9h** at 24 hours post-transfection. Error bars denote the standard error for three replicates.

Figure 6. A) Compound **9h** does not inhibit the appearance of IR-induced RAD51 foci in 293-DR-GFP cells over an 8-hour time course. At least 100 nuclei per condition are represented. **B)** Representative micrographs showing co-localization of RAD51 foci with replication protein A (RPA) foci in DAPI-counterstained 293-DR-GFP nuclei at 8 hours post-irradiation in 293-DR-GFP cells treated with **9h** or the DMSO vehicle control.

Figure 7. A, B) Electromobility shift assay showing RAD51-ssDNA binding in the presence of **9h** or RI-1, respectively. **C)** **9h** does not destabilize RAD51-ssDNA nucleoprotein filaments as

shown by salt titration midpoint. RI-1 serves as a positive control for disruption of RAD51-ssDNA nucleoprotein filament stability. Error bars denote the standard error for three replicates.

D, E, F) Representative D-loop assay gel images showing recombinase-mediated assimilation of a radiolabeled ssDNA oligonucleotide into the homologous region of a supercoiled dsDNA plasmid in the presence of **9h** by human RAD51 protein, *S. cerevisiae* Rad51 and Rad52 proteins, or *E. coli* RecA protein, respectively. Error bars denote the standard error for three replicates.

Figure 8. Clonogenic survival of **A)** U2OS, **B)** PC-3, and **C)** MCF-7 tumor cell lines treated with ionizing radiation followed by outgrowth in the presence of **9h** or the vehicle-only control. Error bars denote the standard error for three replicates.

References

- (1) Thompson, L. H.; Schild, D. Homologous Recombinational Repair of DNA Ensures Mammalian Chromosome Stability. *Mutat. Res.* **2001**, *477*, 131-153.
- (2) Tebbs, R. S.; Zhao, Y.; Tucker, J. D.; Scheerer, J. B.; Siciliano, M. J.; Hwang, M.; Liu, N.; Legerski, R. J.; Thompson, L. H. Correction of Chromosomal Instability and Sensitivity to Diverse Mutagens by a Cloned Cdna of the Xrcc3 DNA Repair Gene. *Proc. Natl. Acad. Sci. U. S. A.* **1995**, *92*, 6354-6358.
- (3) Liu, N.; Lamerdin, J. E.; Tebbs, R. S.; Schild, D.; Tucker, J. D.; Shen, M. R.; Brookman, K. W.; Siciliano, M. J.; Walter, C. A.; Fan, W.; Narayana, L. S.; Zhou, Z. Q.; Adamson, A. W.; Sorensen, K. J.; Chen, D. J.; Jones, N. J.; Thompson, L. H. Xrcc2 and Xrcc3, New Human Rad51-Family Members, Promote Chromosome Stability and Protect against DNA Cross-Links and Other Damages. *Mol. Cell* **1998**, *1*, 783-793.
- (4) Takata, M.; Sasaki, M. S.; Tachiiri, S.; Fukushima, T.; Sonoda, E.; Schild, D.; Thompson, L. H.; Takeda, S. Chromosome Instability and Defective Recombinational Repair in Knockout Mutants of the Five Rad51 Paralogs. *Mol. Cell Biol.* **2001**, *21*, 2858-2866.

- (5) Klein, H. L. The Consequences of Rad51 Overexpression for Normal and Tumor Cells. *DNA Repair (Amst)* **2008**, *7*, 686-693.
- (6) Hine, C. M.; Seluanov, A.; Gorbunova, V. Use of the Rad51 Promoter for Targeted Anti-Cancer Therapy. *Proc. Natl. Acad. Sci. U. S. A.* **2008**, *105*, 20810-20815.
- (7) Vispe, S.; Cazaux, C.; Lesca, C.; Defais, M. Overexpression of Rad51 Protein Stimulates Homologous Recombination and Increases Resistance of Mammalian Cells to Ionizing Radiation. *Nucleic Acids Res.* **1998**, *26*, 2859-2864.
- (8) Slupianek, A.; Schmutte, C.; Tomblin, G.; Nieborowska-Skorska, M.; Hoser, G.; Nowicki, M. O.; Pierce, A. J.; Fishel, R.; Skorski, T. Bcr/Abl Regulates Mammalian RecA Homologs, Resulting in Drug Resistance. *Mol. Cell* **2001**, *8*, 795-806.
- (9) Bello, V. E.; Aloyz, R. S.; Christodouloupoulos, G.; Panasci, L. C. Homologous Recombinational Repair Vis-a-Vis Chlorambucil Resistance in Chronic Lymphocytic Leukemia. *Biochem. Pharmacol.* **2002**, *63*, 1585-1588.
- (10) Hansen, L. T.; Lundin, C.; Spang-Thomsen, M.; Petersen, L. N.; Helleday, T. The Role of Rad51 in Etoposide (Vp16) Resistance in Small Cell Lung Cancer. *Int. J. Cancer* **2003**, *105*, 472-479.
- (11) Russell, J. S.; Brady, K.; Burgan, W. E.; Cerra, M. A.; Oswald, K. A.; Camphausen, K.; Tofilon, P. J. Gleevec-Mediated Inhibition of Rad51 Expression and Enhancement of Tumor Cell Radiosensitivity. *Cancer Res.* **2003**, *63*, 7377-7383.
- (12) Ito, M.; Yamamoto, S.; Nimura, K.; Hiraoka, K.; Tamai, K.; Kaneda, Y. Rad51 Sirna Delivered by Hvj Envelope Vector Enhances the Anti-Cancer Effect of Cisplatin. *J. Gene Med.* **2005**, *7*, 1044-1052.
- (13) Budke, B.; Logan, H. L.; Kalin, J. H.; Zelivianskaia, A. S.; Cameron McGuire, W.; Miller, L. L.; Stark, J. M.; Kozikowski, A. P.; Bishop, D. K.; Connell, P. P. Ri-1: A Chemical Inhibitor of Rad51 That Disrupts Homologous Recombination in Human Cells. *Nucleic Acids Res.* **2012**, *40*, 7347-7357.
- (14) Axelle Renodon-Cornière, Pierre Weigel, Magali Le Breton, Fabrice Fleury. *New Potential Therapeutic Approaches by Targeting Rad51- Dependent Homologous Recombination*. New Research Directions in DNA Repair. Prof. Clark Chen, Ed.; InTech: **2013**.
- (15) Carvalho, J. F.; Kanaar, R. Targeting Homologous Recombination-Mediated DNA Repair in Cancer. *Expert Opin. Ther. Targets* **2014**, *18*, 427-458.
- (16) Huang, F.; Mazin, A. V. Targeting the Homologous Recombination Pathway by Small Molecule Modulators. *Bioorg. Med. Chem. Lett.* **2014**, *24*, 3006-3013.

- (17) Huang, F.; Mazina, O. M.; Zentner, I. J.; Cocklin, S.; Mazin, A. V. Inhibition of Homologous Recombination in Human Cells by Targeting Rad51 Recombinase. *J. Med. Chem.* **2012**, *55*, 3011-3020.
- (18) Ishida, T.; Takizawa, Y.; Kainuma, T.; Inoue, J.; Mikawa, T.; Shibata, T.; Suzuki, H.; Tashiro, S.; Kurumizaka, H. Dids, a Chemical Compound That Inhibits Rad51-Mediated Homologous Pairing and Strand Exchange. *Nucleic Acids Res.* **2009**, *37*, 3367-3376.
- (19) Budke, B.; Kalin, J. H.; Pawlowski, M.; Zelivianskaia, A. S.; Wu, M.; Kozikowski, A. P.; Connell, P. P. An Optimized Rad51 Inhibitor That Disrupts Homologous Recombination without Requiring Michael Acceptor Reactivity. *J. Med. Chem.* **2013**, *56*, 254-263.
- (20) Takaku, M.; Kainuma, T.; Ishida-Takaku, T.; Ishigami, S.; Suzuki, H.; Tashiro, S.; van Soest, R. W.; Nakao, Y.; Kurumizaka, H. Halenaquinone, a Chemical Compound That Specifically Inhibits the Secondary DNA Binding of Rad51. *Genes Cells* **2011**, *16*, 427-436.
- (21) Schlacher, K.; Christ, N.; Siaud, N.; Egashira, A.; Wu, H.; Jasin, M. Double-Strand Break Repair-Independent Role for Brca2 in Blocking Stalled Replication Fork Degradation by Mre11. *Cell* **2011**, *145*, 529-542.
- (22) Ying, S.; Hamdy, F. C.; Helleday, T. Mre11-Dependent Degradation of Stalled DNA Replication Forks Is Prevented by Brca2 and Parp1. *Cancer Res.* **2012**, *72*, 2814-2821.
- (23) Jayathilaka, K.; Sheridan, S. D.; Bold, T. D.; Bochenska, K.; Logan, H. L.; Weichselbaum, R. R.; Bishop, D. K.; Connell, P. P. A Chemical Compound That Stimulates the Human Homologous Recombination Protein Rad51. *Proc. Natl. Acad. Sci. U. S. A.* **2008**, *105*, 15848-15853.
- (24) Budke, B.; Chan, Y. L.; Bishop, D. K.; Connell, P. P. Real-Time Solution Measurement of Rad51- and RecA-Mediated Strand Assimilation without Background Annealing. *Nucleic Acids Res.* **2013**, *41*, e130.
- (25) Cheng, J.; Giguere, P. M.; Onajole, O. K.; Lv, W.; Gaisin, A.; Gunosewoyo, H.; Schmerberg, C. M.; Pogorelov, V. M.; Rodriguiz, R. M.; Vistoli, G.; Wetsel, W. C.; Roth, B. L.; Kozikowski, A. P. Optimization of 2-Phenylcyclopropylmethylamines as Selective Serotonin 2c Receptor Agonists and Their Evaluation as Potential Antipsychotic Agents. *J. Med. Chem.* **2015**, *58*, 1992-2002.
- (26) Cheng, J.; Giguere, P. M.; Lv, W.; Roth, B. L.; Kozikowski, A. P. Design and Synthesis of (2-(5-Chloro-2,2-Dimethyl-2,3-Dihydrobenzofuran-7-Yl)Cyclopropyl)Methanamine as a Selective Serotonin 2c Agonist. *Tetrahedron Lett.* **2015**, *56*, 3420-3422.
- (27) Bennardo, N.; Cheng, A.; Huang, N.; Stark, J. M. Alternative-Nhej Is a Mechanistically Distinct Pathway of Mammalian Chromosome Break Repair. *PLoS Genet.* **2008**, *4*, e1000110.

- (28) Stark, J. M.; Pierce, A. J.; Oh, J.; Pastink, A.; Jasin, M. Genetic Steps of Mammalian Homologous Repair with Distinct Mutagenic Consequences. *Mol Cell Biol* **2004**, *24*, 9305-9316.
- (29) Raderschall, E.; Stout, K.; Freier, S.; Suckow, V.; Schweiger, S.; Haaf, T. Elevated Levels of Rad51 Recombination Protein in Tumor Cells. *Cancer Res.* **2002**, *62*, 219-225.
- (30) Guillon, J.; Grellier, P.; Labaied, M.; Sonnet, P.; Leger, J. M.; Deprez-Poulain, R.; Forfar-Bares, I.; Dallemagne, P.; Lemaitre, N.; Pehourcq, F.; Rochette, J.; Sergheraert, C.; Jarry, C. Synthesis, Antimalarial Activity, and Molecular Modeling of New Pyrrolo[1,2-a]Quinoxalines, Bispyrrolo[1,2-a]Quinoxalines, Bispyrido[3,2-E]Pyrrolo[1,2-a]Pyrazines, and Bispyrrolo[1,2-a]Thieno[3,2-E]Pyrazines. *J. Med. Chem.* **2004**, *47*, 1997-2009.
- (31) Campiani, G.; Morelli, E.; Gemma, S.; Nacci, V.; Butini, S.; Hamon, M.; Novellino, E.; Greco, G.; Cagnotto, A.; Goegan, M.; Cervo, L.; Dalla Valle, F.; Fracasso, C.; Caccia, S.; Mennini, T. Pyrroloquinoxaline Derivatives as High-Affinity and Selective 5-Ht(3) Receptor Agonists: Synthesis, Further Structure-Activity Relationships, and Biological Studies. *J. Med. Chem.* **1999**, *42*, 4362-4379.
- (32) Preetam, A.; Nath, M. An Eco-Friendly Pictet-Spengler Approach to Pyrrolo- and Indolo[1,2-a]Quinoxalines Using P-Dodecylbenzenesulfonic Acid as an Efficient Bronsted Acid Catalyst. *RSC Advances* **2015**, *5*, 21843-21853.
- (33) Guillon, J.; Forfar, I.; Mamani-Matsuda, M.; Desplat, V.; Saliege, M.; Thiolat, D.; Massip, S.; Tabourier, A.; Leger, J. M.; Dufaure, B.; Haumont, G.; Jarry, C.; Mossalayi, D. Synthesis, Analytical Behaviour and Biological Evaluation of New 4-Substituted Pyrrolo[1,2-a]Quinoxalines as Antileishmanial Agents. *Bioorg. Med. Chem.* **2007**, *15*, 194-210.
- (34) Wang, C.; Li, Y.; Guo, R.; Tian, J.; Tao, C.; Cheng, B.; Wang, H.; Zhang, J.; Zhai, H. Iodine-Catalyzed Facile Synthesis of Pyrrolo- and Indolo[1,2-a]Quinoxalines. *Asian Journal of Organic Chemistry* **2015**, *4*, 866-869.
- (35) Cloud, V.; Chan, Y. L.; Grubb, J.; Budke, B.; Bishop, D. K. Rad51 Is an Accessory Factor for Dmc1-Mediated Joint Molecule Formation During Meiosis. *Science* **2012**, *337*, 1222-1225.
- (36) Sikorski, R. S.; Hieter, P. A System of Shuttle Vectors and Yeast Host Strains Designed for Efficient Manipulation of DNA in *Saccharomyces Cerevisiae*. *Genetics* **1989**, *122*, 19-27.
- (37) R Core Team. *R: A Language and Environment for Statistical Computing*, R Foundation for Statistical Computing: **2015**.
- (38) Eklund, A. *The Bee Swarm Plot, an Alternative to Stripchart.*, **2015**.

Figure 1

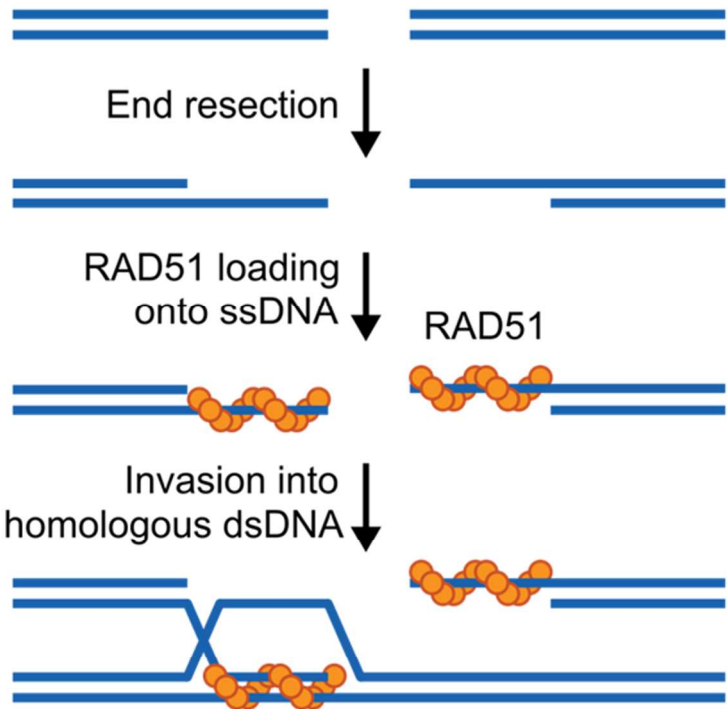


Figure 2

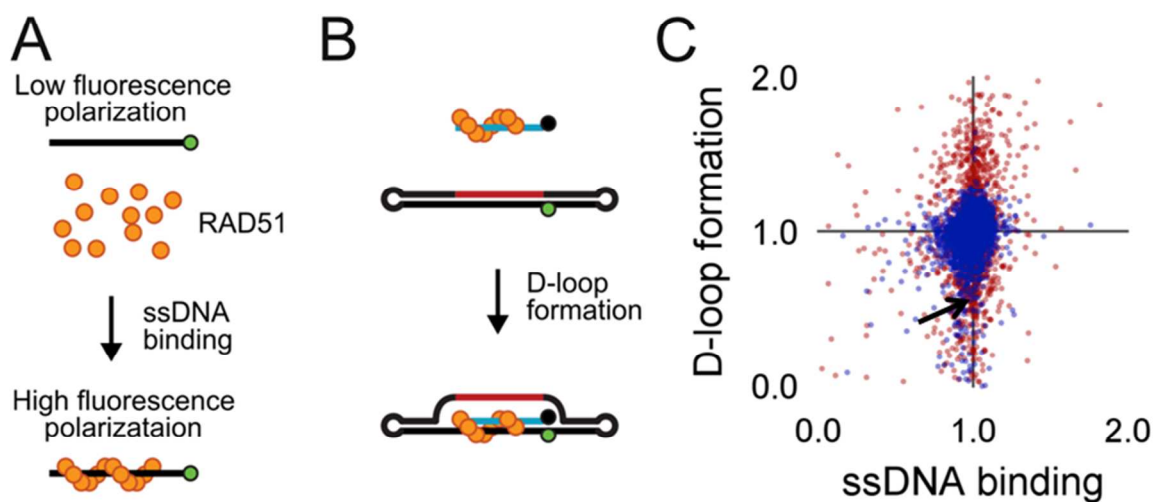
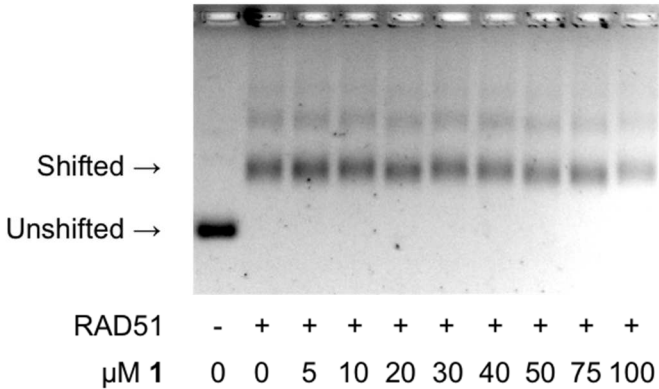


Figure 3

A



B

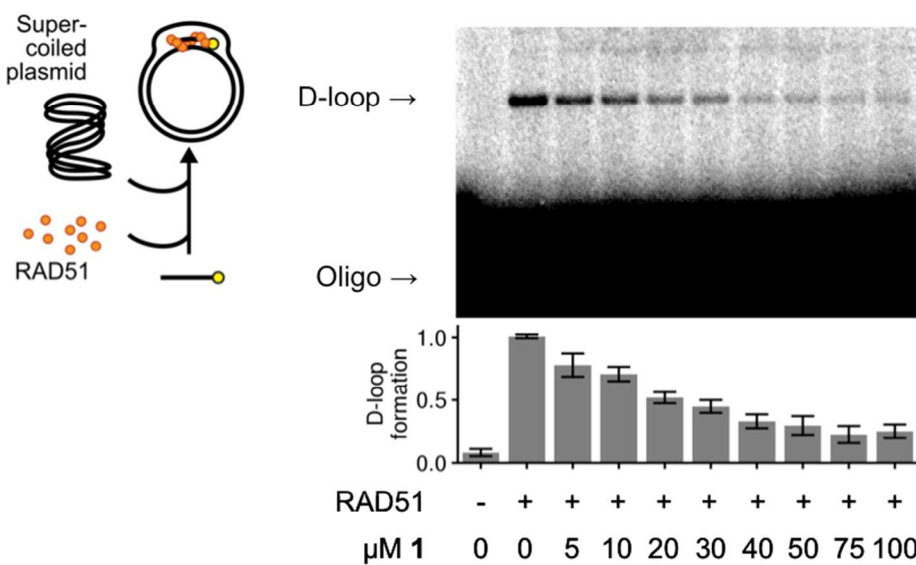
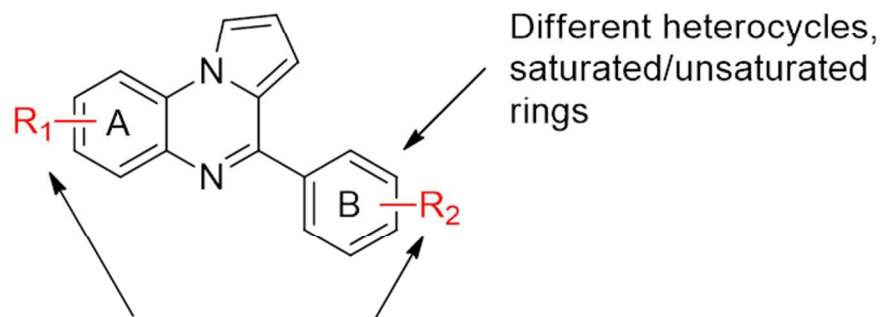


Figure 4



One or more substituents in different positions, including alkyl groups, electron withdrawing/donating groups, hydrogen bond donor/acceptor, etc.

Figure 5

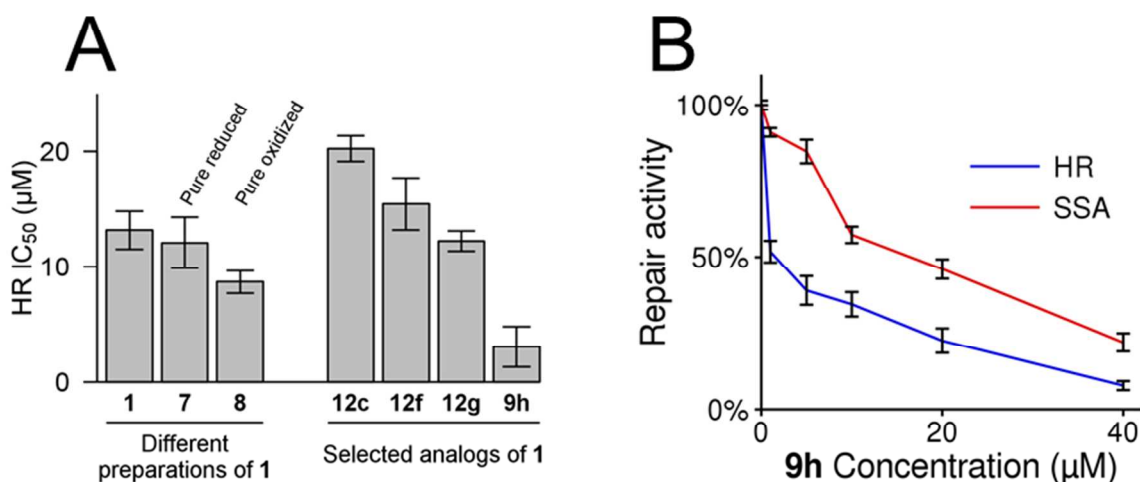


Figure 6

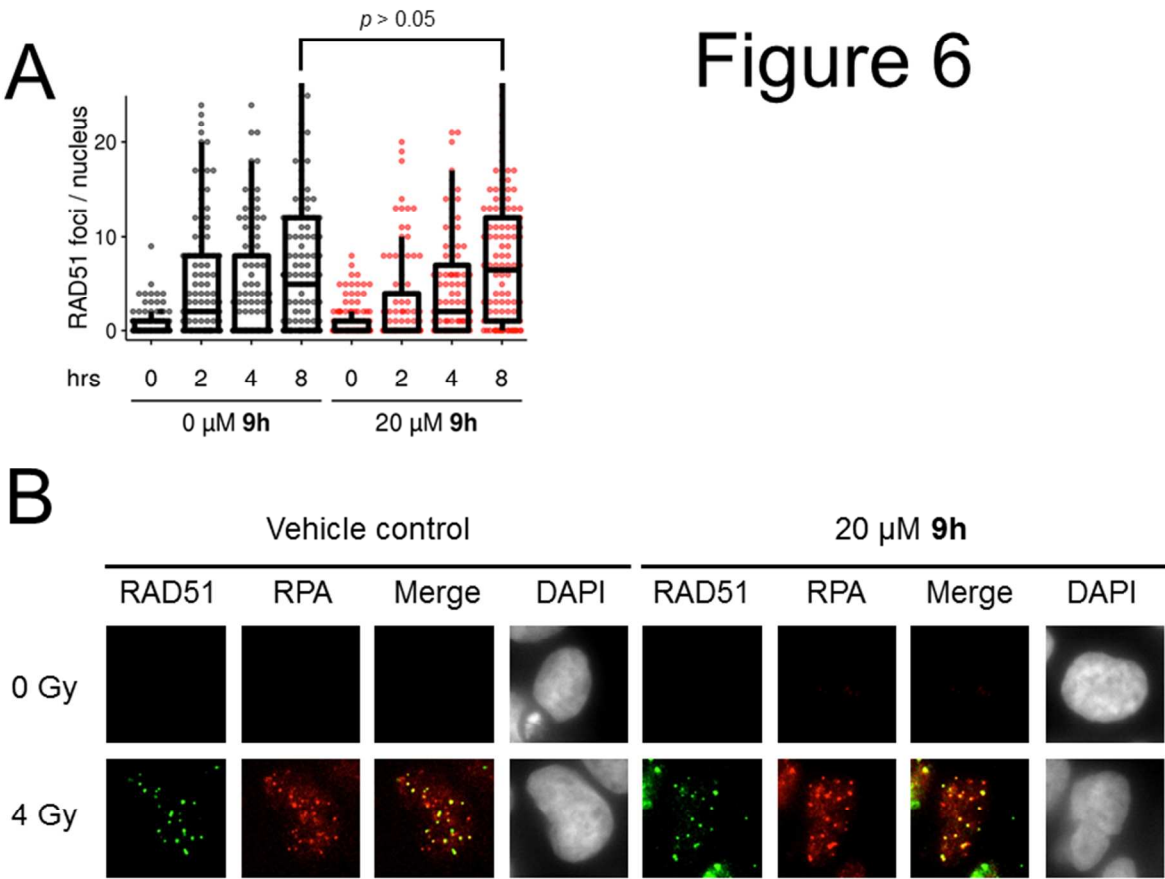


Figure 7

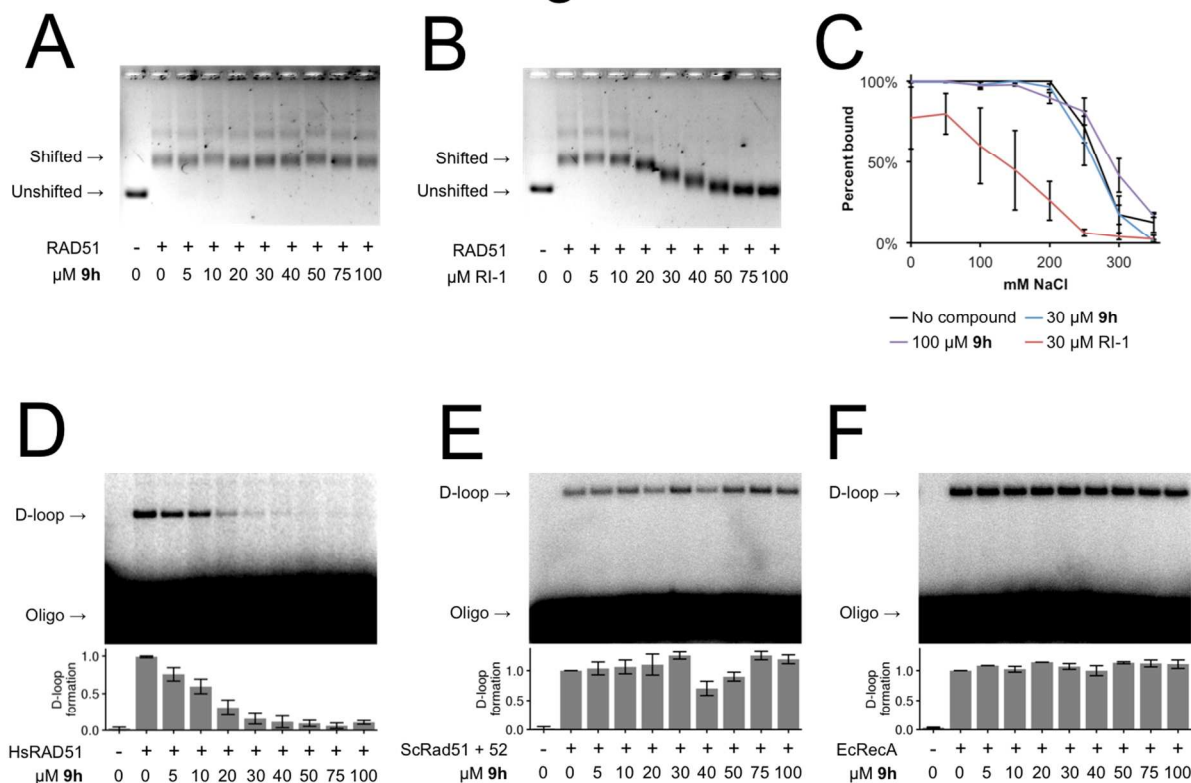


Figure 8

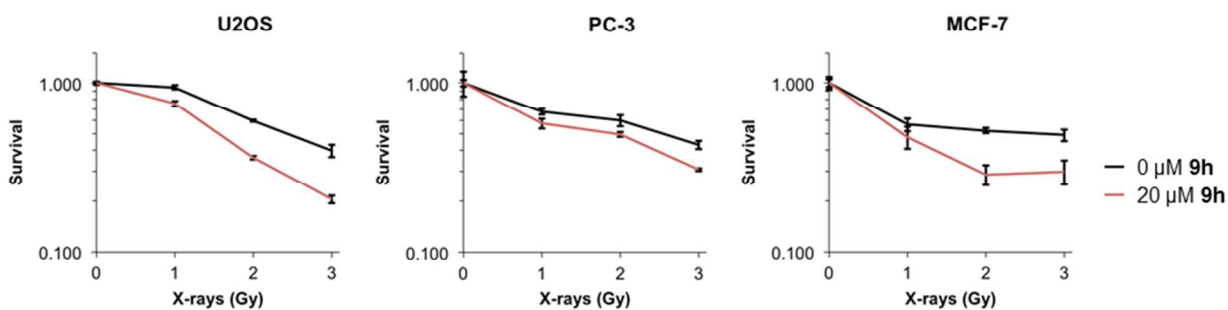


Table of Contents graphic

TOC Graphic

